



Review article

A review of green methods for phyto-fabrication of hematite (α -Fe₂O₃) nanoparticles and their characterization, properties, and applicationsMostafa F. Al-Hakkani^{a,b,*}, Gamal A. Gouda^a, Sedky H.A. Hassan^c^a Department of Chemistry, Faculty of Science, Al-Azhar University, Assiut Branch, 71524, Assiut, Egypt^b Department of Chemistry, Faculty of Science, New Valley University, Al-Kharja 72511, Egypt^c Department of Botany & Microbiology, Faculty of Science, New Valley University, Al-Kharja 72511, Egypt

ARTICLE INFO

Keywords:

Nanoparticles

Biosynthesis

Hematite

Anti-cancer

Anti-microbial

Water purification

ABSTRACT

The aim of the current work is the introduction of a quick and simple literature survey about the bio-fabrication of the Alpha Hematite nanoparticles (α -Fe₂O₃) using the plant extracts green method. The survey manifested the utilities of the environmentally friendly biosynthesis methods *via* extracting different plant species, some of its important physicochemical properties, various instrumental analysis characterization tools, and potential applications.

1. Introduction

1.1. Different types of iron oxide nanoparticles

Most of the transition metal ions like Fe, Co, Ni, and their compounds can be used for the preparation of magnetic nanoparticles (NPs) [1]. Iron is a particular element that can be occurred in diverse forms ranging from zero to three-valence. Additionally, each iron compounds have different characteristics, from magnetic to ferromagnetic. Iron oxides (IOs) coming under magnetic NPs are Magnetite (Fe₃O₄), Maghemite (γ -Fe₂O₃), Hematite (α -Fe₂O₃), and Goethite (FeO(OH)) [1]. Hematite is a thermodynamically more stable mineral than other IOs in the presence of oxygen [2] and exhibits strong electron-electron interactions and electron-photon resonances accompanied by complex electronic structures with interesting optoelectronic characteristics [3].

Hematite is the second common and major IOs. It is isostructural as corundum (α -Al₂O₃) that consists of an intense structure connected to iron III cation in octahedral coordination with oxygen in the hexagonal closed-packing system. The crystallographic system of Hematite is hexagonal with the Miller parameters of $a = 5.0346 \text{ \AA}$ & $c = 13.752 \text{ \AA}$. The structure can be depicted as the stacking of iron III cation layers between two layers of oxygen in the closed-packed system, connecting together by a covalent bond. The structure was shown in a three-dimensional framework developed along with trigonally distorted octahedral FeO₆ associated with thirteen neighbors by one face, three edges, and six

vertices. Because iron is in a trivalent state so, each one of the oxygen is linked with just two iron III cations, and so, just two of three octahedrons of oxygen available are used. This distinctive framework clearly makes the system profitable without any deficit or excess in charge.

Generally, Hematite specific surface area ranges from 10 to 90 m²/g [4, 5]. According to its particular electrical, optical and magnetic properties, the synthesis of α -HNPs has continued to develop in recent decades [6].

1.2. Some of the most common and important activities of iron oxide nanoparticles

1.2.1. The magnetic activity of iron oxide nanoparticles

Iron oxide nanoparticles (IONPs) are categorized according to their response when there are exposed to an externally applied magnetic field. Overview of the magnetic moment orientations in the particle helps to identify the various types of magnetism found in nature. The magnetic properties of such particles can be specified *via* dependence on the magnetic induction B on the applied magnetic field H. Figure 1 and Tables 1 and 2 summarized the classification of materials according to their magnetic behavior [7, 8]. Some materials like iron exhibit ferromagnetism that can be magnetized permanently. The relationship between most materials B and H is linear: $B = \mu H$; where μ is the particle magnetic permeability. IOs show paramagnetism if $\mu > 1$; and diamagnetism if $\mu < 1$. In vacuum, $\mu = 1$. Alternatively, the magnetic susceptibility $\chi = \mu - 1$ is

* Corresponding author.

E-mail address: mostafa.f@scinv.au.edu.eg (M.F. Al-Hakkani).

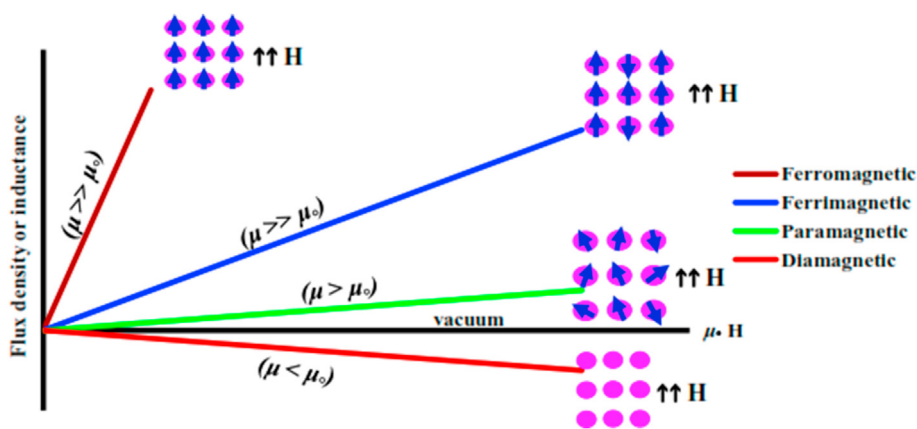


Figure 1. Permeability and different magnetic materials.

Table 1. Classification of magnetic behavior for different materials.

Material type	Example	Atomic moment	Susceptibility
Diamagnetism	Inert gases He, Ne, Ar, Kr, Xe, Rn Metals as Cu, Ag, Au, Hg Non-metals as B, P, S Ions as Na^+ , Cl^- Molecules as H_2 , N_2 , H_2O Organic compounds	No magnetic moment	Small and negative About $[-10^{-6}$: $-10^{-5}]$
Paramagnetism	Metals as Na, Al, Ca Ions as transition metals and rare earth metals Molecules O_2 Oxides as rare earth elements	Randomly oriented magnetic moment	Small and positive About $[10^{-5}$ to $10^{-3}]$
Ferromagnetism	Transitions metals as Fe, Co, Ni Some alloys of Mn as MnBi, Cu_2MnAl	Parallel aligned magnetic moments	Larger
Ferrimagnetism	Magnetite (Fe_3O_4) Mixed oxides of iron with other elements such as Sr ferrite ($\text{SrFe}_{12}\text{O}_{19}$ ($\text{SrO} \cdot 6\text{Fe}_2\text{O}_3$))	Mixed parallel and antiparallel aligned magnetic moments	Large
Anti-ferromagnetism	Transition metals as Mn, Cr Transition metals compound as MnO, CoO, NiO, Cr_2O_3 , MnS, MnSe	Antiparallel aligned magnetic moments	Small and positive About $[10^{-5}$ to $10^{-3}]$

used. Hence, paramagnetic NPs have $\chi > 0$; diamagnetic particles $\chi < 0$ and in vacuum $\chi = 1$ [9].

The important distinctive characteristic for the magnetic NPs is superparamagnetic, which provides high stability and better dispersion when the magnetic field is eliminated since there is no residual magnetic force between the particles. When the NPs are so small below around 15 nm that the cooperative ferromagnetism tendency is no longer observed and no permanent magnetization is available after the particles have been exposed to an external magnetic field. The particles, however, still exhibit very high paramagnetic properties with very high susceptibility [10].

Particles whose unpaired electron spins are randomly coordinated to enable the substance to manifest magnetism without being under a magnetic field are termed ferromagnetic particles. Ferromagnetism is such a collaborative effect because single atoms cannot manifest ferromagnetism, but once a sufficient amount of atoms are strongly coupled together, ferromagnetic properties occur. We can observe permanent magnetization when the ferromagnetic particles are excluded from the magnetic field. Ferromagnetic materials, which are near to particle dimensions smaller than a specified range, are no longer ferromagnetic but show super paramagnetism [11].

If a particle includes magnetic moments that can be associated with an external magnetic field, this amplifies the field. These substances demonstrate paramagnetism properties. On contrary to ferromagnetic materials (ferromagnetism), after shielding the materials from the magnetic field, no permanent magnetization occurs in paramagnetic

material. Paramagnetism can be described by presupposing eternal atomic magnetic moments that can be reoriented during an external field. These moments may be either due to electron orbiting, or attributable to the atomic nucleus. The torque applied to these moments by the external magnetic field helps to align them parallel to the field, which then follows reinforces it [9]. Sato *et al.* proposed that magnetization loss as particle size decreases is largely dependent on the energy constant of the crystalline magnetic anisotropy, K . Smaller K constant shows lower relative values of magnetization [12].

Super paramagnetism analyzes including microscopic, XRD, and magnetometry studies suggest the decreased magnetization is attributed to surface characteristics of the NPs. The lack of magnetization may be directly attributable to the presence of a dead magnetic layer at about a thickness of 1 nm caused by an asymmetric impact of the surface atoms [12]. Lastly, investigations using spectroscopic analysis indicated a spin-canting surface effect and had declared to be improved as the particle size and temperature decreased [13].

Particles synthesized from IOs tend to behave differently depending on their size in the magnetic field. It was previously reported by several researchers [14, 15] the dramatic shift in magnetic properties arises when the particle size is decreased from micrometer to scale of a nanometer. Particles as superparamagnetic materials, when the size is small enough (i.e. 6-15 nm) and they behave as ferromagnetic when the grain size is in the micrometer range. Chatterjee *et al.* [16] reported that the blocking temperature of the particles depends on magnetic conduct (Blocking temperature is the transition temperature directly proportional

to the particle size, between the ferrimagnetic and superparamagnetic states), that in essence, depends on the size of the particles. Particles of lower freezing temperature showed superparamagnetic properties, while the higher blocking temperature of the particles revealed the ferromagnetic nature. Although increasing in the superparamagnetic attitude of particles with lower particle size, several authors recorded decreasing in exacted magnetization values of saturation when the particle size is lessened to less than 10 nm [17, 18].

Modification of the surface for the IONPs commonly results in the creation of a non-magnetic surface owing to the deposition of an outer layer of particles and the thickness of such a layer could be 1–20 nm [19].

The coating of particles with non-magnetic materials will lead to decreasing in the magnetization values. Gomez-Lopera *et al.* [20] & Voit *et al.* [21] reported that the surface coating of poly (lactide-co-glycolide) polymer on IONPs was observed to decrease the magnetization of particles to around half that of pure magnetite and the initial magnetization–magnetic field dependence, in this case, is steeper. Voit *et al.* [21] conducted the superparamagnetic IONPs' magnetic activity in ferrofluids coated with different polymers, such as sodium oleate, polyvinyl alcohol (PVA) starch. They observed that the IONP's surface coating with either of these polymers resulted in decreasing in saturation magnetization values (M_s) of the particles. They also observed that the values of particle sizes determined from the magnetization data were smaller than those of the values calculated by XRD and TEM measurements, which may be assigned to a magnetically ineffective layer on the particle surface [22]. Weak ferromagnetism below the Morin transition at 260 K for α - Fe_2O_3 NPs with truncated hexagonal bipyramidal morphology is shown due to the high surface energy of the exposed (101) and (001) facets [23].

1.2.2. Electric activity of IONPs

As the most stable IOs and n -type semiconductors under long term conditions, α - Fe_2O_3 are widely used as catalysts, pigments, and gas sensors due to their low cost and high corrosion resistance. It may also be used as a starting substrate for magnetite synthesis (Fe_3O_4) and maghemite (γ - Fe_2O_3), which intensively sought both for basic scientific interests and for technical uses in the last few years [24]. Hematite is an n -type semiconductor with an energy band gap in the range 2.1–2.3 eV [25, 26], where the conduction band is composed of empty d-orbitals of Fe^{3+} and the valence band consists of occupied 3d crystal field orbitals of Fe^{3+} with some admixture from the O 2p non-bonding orbitals [25].

1.2.3. Biological activity of IONPs

Indeed, the biological properties of NPs are strongly associated with the physio-chemical nature of NPs as well as the capping molecules employed in salt precursor reduction and on the surface of NPs immobilize. The most probable explanation is the usage of biological products in the production of NPs, such as phenols, aldehydes, ketones, reducing acids, alkaloids, flavonoids, and, or, etc. The free radical scavenging efficacy has a direct relationship to antioxidant properties as well as behavior-like phenolic and flavonoid molecules [27, 28, 29].

The bioactive constituents adhered to the surface of the NPs are responsible for these efficacies. Likewise, these properties are also related to the biological applications of NPs. The mildly radical scavenging behavior is effective in the struggle against oxidative stress whereas the low quantification present of phenolic and flavonoid ingredients during biological applications does not have any extra cell burden [30].

There are two potential pathways proven against Gram-positive or Gram-negative bacteria for the α -HNPs as an antibacterial agent. As these

Table 2. Atomic/magnetic behavior before and after applying the magnetic field.


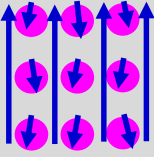
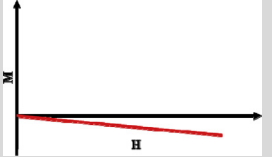

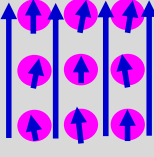
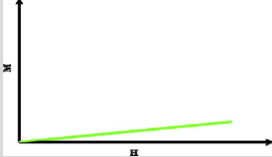
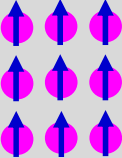
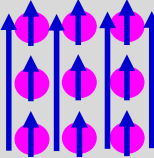
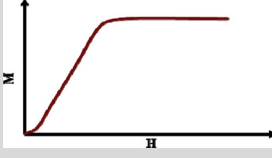
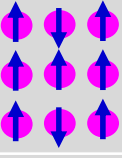
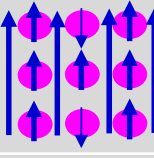
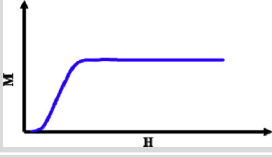
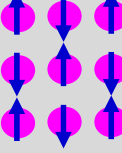
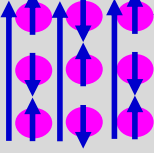
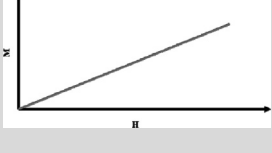
Material type	Before	After	Curve
Diamagnetism			
Paramagnetism			
Ferromagnetism			
Ferrimagnetism			
Anti-ferromagnetism			

Table 3. Adsorption maximum capacity survey of α -HNPs against different adsorbates for water treatment.

Adsorbate	Maximum capacity (mg/g)			Ref
Cephalexin	70			[68]
Acetylsalicylic acid	60.189			[69]
As (V)	75.3			[70]
	7.6			[71]
	51			[72]
Congo red dye	160			[70]
	53			[73]
	66			[74]
Heavy metals	pH			[75]
	4	6	8	
	Pb	4.69	7.24	120.00
	Cd	31.20	37.40	263.00
Cu	46.00	84.80	98.40	
Zn	10.30	13.30	131.00	
Asphaltene	29.97			[76]
Cr (VI)	200			[77]

α -HNPs are extremely stable in the atmospheric environment, there is less contribution to antibacterial activity from the release of the metal ion. Through comparison, UV promotes the generation of reactive oxygen species that are produced from the defect sites of α -HNPs or visible light electron-hole pairs. The electron-hole pairs that have been produced will help generate reactive oxygen species such as superoxide radical anions ($O_2^{\bullet-}$), hydroxyl radicals ($\bullet OH$), etc. [31]. Besides, various interactions such as electrostatic, dipole-dipolar, hydrogen bond, hydrophobic, and *Van der wall* interactions are responsible for disrupting the cellular structure and disrupting and disorganizing membranes [32].

Reduction potential determination of the plant extract considers a convenient tool to confirm the reduction role of the polyphenols and flavonoids present in the plant extract. Where it determines the ability to reduce the metal ions precursor as in our case study of iron, where the standard reduction potential is 0.44 V [33]. This reduction process is spontaneous and conceivable if the reduction potential of the used plant extract is located at the standard reduction potential of the polyphenols in the leaf extract 0.534–0.540 V [34]. The capping organic constituents especially polyphenols and flavonoids cause an increase in the surface charge of the formed NPs and thus stability enhancement was achieved by aggregation inhabitation [35].

1.2.4. Antimicrobial activity of IONPs

Over the last three decades, where traditional pharmaceutical methods have been widely used for antibacterial and antifungal therapies. This allowed these microorganisms to mutate and reproduce the new medium to continue with its adaptability and life. But, to combat the current conventional therapies, these microorganisms are in continuous production on their own. Scientists researching solutions thus have to actively study for best and safer ways to suppress and remove these microorganisms in their new type. Many recent aspects of studies have included the use of gold, silver, and iron NPs/NMs to be used by Gram-positive and Gram-negative bacteria as a wide spectrum antibiotic. Studies have also been developed and applied to include the use of such α -Fe₂O₃ NPs as an antifungal for different organisms [32, 34, 36, 37, 38, 39, 40, 41].

1.2.5. Anticancer activity of IONPs

Studies for some elements began involving almost all of the nanoparticles (NPs). The study launched with Au NPs in-vitro experiments to be used as an aid in the treatment of some forms of tumors and cancers [42]. The studies manifested predictions that were very promising in these fields. Continuous progress has not yet stopped concurrently seeking healthy, sustainable, and economical approaches, beginning

with the synthesis of these particles in an environmentally-friendly route. Therefore, observations in the use of these NPs have been replicated as shown by laboratory work attributable to their lethal properties for some of those diseases. IONPs have not frequently been the center of concern relative to Au NPs and Ag NPs, but they are now the field of interest for most researchers and scientists due to the characteristics that allow them to succeed in this region. Many trials of α -Fe₂O₃ NPs have been encouraging for use as an option in the treatment of some tumors and specific cancers [2, 30, 43, 44, 45, 46].

1.2.6. Purification and aquatic environment treatment

Several types of fabricated nanomaterials (NMs) have been developed and are encountering applications in diverse areas, from personal care products to large-scale composites of structures. The unique, special physicochemical and surface properties of the ultra-scale NMs were used to create groundbreaking approaches to many daunting environmental issues. Significant efforts are ongoing to improve and investigate the uses of NMs in applications such as membrane isolation, catalysis, adsorption, sensing, and processing with a view to improved environmental safety [47, 48]. NPs of many metals and metal oxides give some good kinetics and improved sorption or catalytic ability for many environmental-significant reactions because of their incredibly high surface area to volume ratio. Metal oxide NPs such as Al (III), Ti (IV), Fe (III), and Zr (IV) oxides are biologically friendly and have amphoteric sorption behaviors. They can serve as Lewis acids (electron acceptors) or bases (electron donors), depending on the pH. Consequently, they can bind transition metal cations including Cu²⁺, Pb²⁺, Zn²⁺, and Ni²⁺; and anionic ligands, including phosphate and arsenate. Since the sorption sites primarily occur on the surface, due to their high area-to-volume ratio, the metal oxides give very high particular sorption potential at nanoscale sizes [49].

1.3. Some of the applications for the magnetic NPs

Noble NPs could be used as catalysts for organic degradations and transformations but it is difficult to separate these NPs from the mixture of reactions and remains a significant task. A lot of researches has been conducted on the processing of magnetic NPs to solve the above major problems. Recently, magnetic NPs have emerged as sustainable, effective, and readily accessible alternatives to traditional materials and are used for various organic degradation/transformation as heterogeneous catalysts [50].

IONPs are of relevance to the researchers because of their unique electromagnetic property, optical property, etc. In addition to these

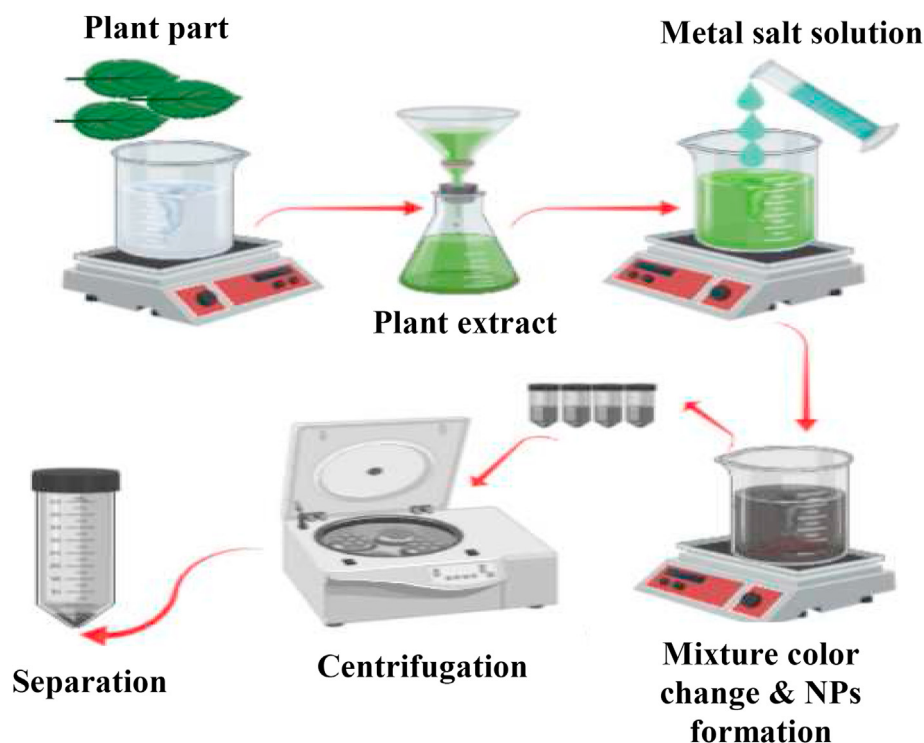


Figure 2. Simple green biosynthesis scheme of nanomaterial formation.

properties due to the other considerations such as low cost, adequate availability makes it more useful for different applications.

Generally, α -HNPs can be used in photocatalytic, gas sensors, lithium-ion batteries, photoelectrochemical cells, and humidity sensors due to properties such as high corrosion resistance and semiconductor [43]. Several application included using of magnetic NPs as, cellular labeling/cell separation [51, 52, 53, 54], detoxification of biological fluids [55, 56], tissue repair [57], drug delivery [16, 58, 59, 60], magnetic resonance imaging [61], hyperthermia (heat) in the treatment of malignant tumors [62], magnetofection [63], cytotoxicity [64], antibacterial and UV protection effect [65], wet-type solar cell [66].

Also, α - Fe_2O_3 has been considered for a wide variety of uses, as it is readily available, non-toxic, and environmentally safe, hardly influenced by oxidation changes [26].

Over the last decade, increased studies have been carried out of many forms of IOs in the magnetic field NPs (including the Fe_3O_4 magnetite, iron II&III oxides mixture, ferrimagnetic, superparamagnetic when its particle size is less than 15 nm), γ - Fe_2O_3 (Maghemite, ferrimagnetic), α - Fe_2O_3 (Hematite, weakly ferromagnetic or antiferromagnetic), FeO (Wüstite, antiferromagnetic), (ϵ - Fe_2O_3 and β - Fe_2O_3) [67].

The green methods alternative in NPs preparation are fairly simple, effective, and environmentally sustainable, as it minimizes the environmental hazards by using non-toxic, recycled materials due to their greater surface-volume ratio.

The synthesized α -HNPs have been directed to use as a catalyst or adsorbent agent to minimize or eliminate the high toxicity materials like dyes, pharmaceuticals, heavy metals, and industrial wastes as shown in Table 3.

1.4. Different preparation methods of α -HNPs

α -HNPs may be synthesized from physical, chemical, or biological routes using many methods. Sol-gel [78, 79], emulsion precipitation-calcination route [80, 81], bacterial growth [82, 83], thermal decomposition [23, 84], laser ablation [85, 86], vapor-solid

growth techniques [87, 88], self-assembly method [65, 89], hydrothermal method [90, 91], biosynthesis “protein capping” [92, 93].

These processes, nevertheless, typically require special equipment, extreme pressure, and temperatures, templates, or substrates, which experience difficulties with prefabrication and post-removal of the templates or substrates and generally lead to impurities that are worse, toxic byproducts.

1.5. Importance of the green chemistry in IONPs preparation

Green chemistry can be defined as “A set of principles which decreases or eliminates using or formation of hazardous substances in the manufacturing design, and chemical products application [94, 95].

The principles of green chemistry can be summarized as mentioned in 1998 by Anastas and Warner at 12 points as the following [94]:

- ▶ Minimization of waste generation.
- ▶ Increasing the amount of desired production yield against the amount of production waste.
- ▶ Employing less hazardous synthetic methods.
- ▶ Designing the chemical products that keep their function without toxic effects.
- ▶ Implementation of solvents that minimize overall toxicity effects within chemical reactions.
- ▶ Enhancing energy use as processing at ambient conditions if possible for example low temperature.
- ▶ Synthesis significant source of chemicals and fuels that reduce the risk of loss.
- ▶ Usage reduction from derivatives such as blocking groups.
- ▶ Accuracy selection in catalytic reagents to use.
- ▶ A toxic-free, degradable chemical design.
- ▶ Using the real-time analysis to monitor the hazardous material formation manufactured.
- ▶ Reduce potential accidents by using more saver chemical reagents.

1.6. Advantages of the use of plants over other green methods as bacteria and fungi

Utilization of plants has many advantages such as no need for preparation of culture media and isolation maintenance, economic, environmentally friendly, safe, stable and non-toxic, short production times for synthesis, and easily scaled up for large-scale production of nanomaterials. Moreover, the most important effective role as a reducing-coating-stabilizing agent in the ambient conditions, and also there is no need for high temperature as in hydrothermal methods [96].

The stability of the synthesized nanoparticles is a vitally important demand in the processing and storage of ferrofluids. Organic compounds are also used to passivate the surface of the IONPs to prevent agglomeration before or during the preparation process. Hydrophobic surfaces with a high surface-area-to-volume ratio are the key causes for magnetic IONPs because there is no sufficient surface coating, and the hydrophobic interactions between the NPs can allow them to accumulate and form large clusters, contributing to increased particle size. Also, some bioactive molecules are often used to improve their biocompatibility. The bioactive molecules may be hydroxylic groups, aldehydic groups, carboxylic groups, amino groups, etc. The source of these organic constituents may be such as polymers, vitamins, proteins, amino acids, liquid plant extracts, sugars, etc. Similar to other biological routes such as yeast, bacteria, algae, and fungi, plant extract has many economic advantages including reduced period and removal of the tedious cycle such as cell culture maintenance. The plant extract approach has gained growing attention in nanotechnology due to its low-cost, high-efficiency, non-toxicity, and eco-friendly characteristics. Green chemistry conducting in nanotechnology including uses of plant spices and herbs has elevated levels of the active antioxidant, terpenoids, alkaloids, flavonoids compounds including the reduction of metal ions precursor as carbohydrates, polyphenols, nitrogen bases, and amino acids, surges. Synthetic methods for plant extract can be sufficiently scaled up for large-scale manufacturing; the process can also be commercially feasible.

The biosynthesis of NPs has been regarded in recent years as a more biologically friendly, sustainable, greener, and cost-effective alternative to chemical and physical processing methods. To extend the researches and applications of the IONPs for biological activity [67].

Considerable efforts have been dedicated in the last decades to the design and regulated processing of nanostructured materials with new complex functional properties. Bioactive molecules especially present in the different plant extracts were being treated for IONPs made to provide high potential use in many fields, especially for good bio-compatibility applications. Figure 2 can summarize the biosynthesis method of a nanomaterial as a general green route for the synthesis of the nanomaterial.

1.7. Biosynthesis mechanism of nanomaterial

Generally, the basic mechanism of formation for the NPs, which include nucleation and particle formation *via* plant extracts, is not recognizable till now. But there are a few appreciate suggestions that were being introduced for the formation mechanism interpretation that depending on complex formation after reduction/oxidation reaction for the iron ions at the first [97, 98, 99]. However, studies indicate that the phytoconstituents (primary and secondary metabolites) in the plant extract play a significant role in the biosynthesis of NPs. In particular, these compounds, as (polyphenols, proteins, flavonoids, tannic acids, terpenoids, alkaloids, sugars, amino acids) especially contain carbonyl, hydroxyl, and amino groups or rich *via* electron cloud groups that act as natural antioxidants to reduce carcinogenic metal ions to NPs [35, 47, 96, 99, 100, 101, 102, 103, 104, 105, 106, 107, 108].

FTIR spectroscopy technique was mostly conducted to investigate the responsible bioactive constituent molecules for the formation of the nanomaterial. All the obvious results confirming that the effective role of the phytoconstituents in the formation of the nanomaterials. This can be

realized by comparison the sharing of the similar function groups that present in the plant extract and that were be found in the formed nanomaterials. These organic bioactive constituents have a great impact on the reduction, stabilization, and capping processes on the surface of the as-biofabricated nanomaterials and improve the physicochemical properties of the later [41, 43, 96, 109, 110, 111, 112, 113].

According to a lot of the diversity of the contents of the bioactive constituent molecules that present in deferent plant extracts; the morphologies and size of nanoparticles were varied [96].

2. Characterization and instrumental and method analysis

Recently, the scientific research has been primarily directed to ensure the precision and accuracy of the results and their validity in terms of repeatability, robustness, and rigidity for the need to keep track and to carry out periodic maintenance requirements for the analysis instruments through calibration and the validation implementation for using of the analysis methods, according to specific rules, conditions and regulations and standard operating procedures [114, 115, 116, 117, 118].

Many techniques of instrumental analysis maybe use under the characterization section as the following:

2.1. Formation of NPs

UV-Visible spectroscopy can be helpful in the measurement of the characteristic surface plasmon resonance in the range of 200–800 nm [107].

2.2. Extraction of NPs

Different separation methods maybe use as direct precipitation, Buchner filtration, and centrifugation [119].

2.3. Surface morphology structure and particle size analysis

Particle size in nanoscale and morphology are parameters of critical importance for NP formation and applications. This can be achieved using many techniques as scanning electron microscopy (SEM) [120] and Atomic force microscopy (AFM) [121] for size and morphology studying, Dynamic light scattering (DLS) [122] for the geometry of NPs study, and size distribution determination and quantify the surface charge of NPs suspended in a liquid, Transmission electron microscopy (TEM) [123] also used for shape and particle size determination.

2.4. Optical and electrical properties of nanoparticles

As mentioned previously; Uv-vis used in optical propertied determination as band gap, transition type determination (direct or indirect; allowed or not allowed) [107, 124], Fourier transform infrared (FTIR) [47, 125] used for identification and functional groups determination that associated with NPs as –OH; –NH; –C=O; –CO; –C=C; –CH groups, etc..., Photoluminescence (PL) is an important method for estimating semiconductor purity and crystallinity performance and disorder amount estimation present in the lattice structure. Photoluminescence has a wide variety of uses including energy band gap estimation, level of impurities, and identification of defects, understanding of the mechanism of recombination, quality monitoring of materials, molecular structure, and modeling of the crystallinity [96].

2.5. Surface charge determination

Stability of the formed NPs which indicates the potential application that may be used. It can be easily determined using Zeta potential that measures the NPs colloidal stability, surface charge, and surface hydrophobicity [120].

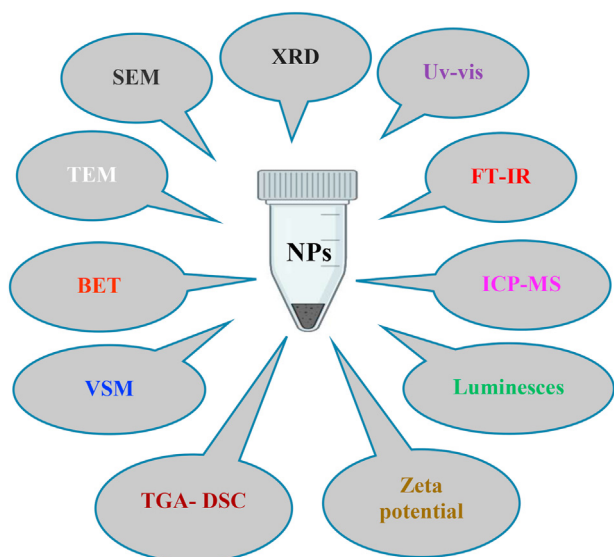


Figure 3. Different and common instrumental analysis tools used in NMs characterization.

2.6. Thermal properties

Thermal analysis (TA) is used with time and temperature to determine the chemical and physical properties of any sample as a mass loss against temperature increasing as Thermal Gravimetric Analysis (TGA). Differential Scanning Calorimetry (DSC) used for measuring the heat released (endo or exothermic reactions) can be realized thoroughly heat changed transformations [124].

2.7. Chemical composition analysis

Energy dispersive spectroscopy (EDS) mapping that determines the elemental composition of NPs [126] and inductively coupled plasma mass spectrometry (ICP-MS) for determination of elemental analysis [116].

2.8. Structure analysis

Powder X-ray diffraction (XRD) used for purity; crystallinity, crystallographic system, and particle size determination from Bragg's law [47, 96, 107].

2.9. Magnetic properties

Vibrating Sample Magnetometry (VSM) can be used for the magnetic behavior of NPs to determine the property of paramagnetism or diamagnetism. It gives more data about the material type if it is strongly attracted by the magnet or magnetic field classified as a (Ferromagnetic materials) if the material is not strongly attracted to the magnet is known as (paramagnetic material) but if it has been found in a strong magnetic field and magnetized if the material repelled against the magnet; it considers as a (Diamagnetic material) [127].

Figure 3 is a simple diagram that shows the most common and important instrumental analysis tools for nanomaterial characterization.

3. Biosynthesis of α -HNPs using different plant extracts and their applications

According to our investigated literary survey that we have, Bashir and his co-workers are considered to have the forefront in the field of green preparation for α -HNPs in 2013 using plant extract. The studies and

researches have been begun and carried out to develop scientific researches production in this exploration area.

Bashir et al. [66] issued their paper entitled "Green synthesis of mesoporous hematite (α -Fe₂O₃) NPs and their photocatalytic activity" using the extract of green *Tea* (*Camellia sinensis*) leaves. SEM analysis demonstrated that the product consists of NPs with sizes ranging from 40–80 nm, also some aggregated particles of size around 100 nm were observed; while TEM revealed that the particles were found to be spherical in shape and pores. The resultant data of XRD were found to be identical with the α -HNPs rhombohedral pattern with high crystallinity when the bio-synthesized NPs were be annealed at high temperatures up to 180 °C. The average crystal size for the as-prepared α -HNPs was calculated and found to be about 33 nm using Debye-Scherrer's equation. Thermal profile and stability were evaluated using TGA manifesting mass constant beyond 400 °C to 700 °C. Four absorption peaks were appeared in UV-Vis-NIR spectrum 290–310 nm, 485–550 nm, 640 nm, and 900 nm, moreover, the absorption intensity of the first two absorption peaks which assigned to the formation of α -HNPs. The surface area of as-prepared α -HNPs was found to be 22.5 m²/g which found that higher than commercial hematite 6 m²/g with Four times. The photocatalytic activity was conducted under visible light irradiation for terephthalic acid indication the ability of the as-biosynthesized α -HNPs as a superior catalyst. Also, the as-prepared α -HNPs were successfully applied in the wet-type solar cell.

The research paper survey was conducted within the period 2014–2020, which was interested in the use of different plant extracts for various parts of the plant for synthesis of α -HNPs. The dependence for the iron metal ion precursors reduction processes was in whole or in part of the organic components present in plant extracts like polyphenols, flavonoids, and other bioactive constituents as well as the primary role of using them as capping or stabilizing for the obtained NPs.

In 2014, in two separate experiments; *Curcuma* and *Tea* leaf extract were used by Alagiri and Hamid [128] as a reductant and stabilizer agent to synthesize α -HNPs. Based on XRD resultant data for each sample, the as-synthesized material confirmed to pure crystalline α -HNPs rhombohedral phase, the crystallite size was evaluated by Debye-Scherrer equation and it was found to be 4 and 5 nm as *Curcuma* and *Tea* leaves extract α -HNPs respectively. The morphology was investigated using SEM analysis revealing similarity in spherical-like shape with uniform size distribution for each sample. For α -HNPs prepared using *Curcuma*; the UV-Vis absorption spectrum was checked and manifested three absorption peaks at 561, 442, and 272 nm whereas the α -HNPs prepared using *Tea* leaves extract revealed absorption peaks at 551, 430, and 272 nm. The direct optical band gaps were calculated and found to be 2.2 and 2.25 eV for the prepared α -HNPs using *Curcuma* and *Tea* leaves extract respectively. According to FT-IR results, the possible mediation of polyphenols, flavonoids, and other expected biomolecules in the synthesized NPs have been understood. Photocatalytic activity of the visible light irradiation using α -HNPs as a catalyst for methyl orange pollutant aqueous solution degradation was conducted giving a very satisfying performance for getting rid of the organic contaminant.

Debasis Nanda in 2015 [129] introduced his master thesis entitled "Green Synthesis of IONPs" where he reported that the ability to prepare α -HNPs using green *Tea* leaf extract. FT-IR analysis of the green *Tea* extract and the as-prepared NMs was conducted to ascertain the capping function of the organic constituents present in the extract to be adsorbed on the NMs. The nature of the as-prepared NMs morphology also has been studied using TEM & FESEM which assure the rod-shaped merit, diameters of the formed rods were determined and found to be in the range 130–150 nm for length and 20nm for width. XRD characterization was investigated for the as-prepared NMs, α -HNPs in the crystalline phase with an average crystal size of 28.9 nm using the Scherrer equation was to be realized.

Also in the same year, Atta et al. [44] used the thermal decomposition (calcinated at 600 °C) of the ferric green synthesized complexes of hippuric acid, itaconic acid, and tyrosine amino acid to synthesize α -HNPs.

The XRD data indicated that a single-phase α -HNPs formation particle size ranging from 20 to 60 nm. They reported that the SEM images of the synthesized α -HNPs are dependent on thermal decompositions which appeared as uniform spherical and hexagonal shapes with particles size 5–50 nm. TEM morphologies of synthesized NPs using thermal decomposition also were conducted which revealed as spherical NPs in the range 5–50 nm in harmonization with the resultant SEM data. The cytotoxic activity against the breast carcinoma cells (MCF-7 cell line) was studied and IC_{50} was found to be within the 3.10–3.81 $\mu\text{g}/\text{mL}$. The characteristic spectrum for the synthesized NPs was investigated using FT-IR which revealed about at range below 750 cm^{-1} .

Muthukumar et al. [35] studied the biogenic synthesis of α -HNPs using *Amaranthus dubius* leaf extract as a reducing agent in 2015. Results showed that *Amaranthus dubius* extract mediated NPs are spherical with a cubic phase structure and a diameter range from 43 to 220 nm with less aggregation. XRD analysis indicated that synthesized NPs were rhombohedral crystalline in structure. An absorption peak at 214 nm was investigated at acidic extract pH 4 where the absorption peak was shifted to 300 nm due to agglomeration of NPs at basic extract pH 9. SEM image showed a sphere-like morphology with less aggregation and sizes that approximately range 60–300 nm. *Amaranthus dubius* mediated α -HNPs for decoloration efficiency against methylene orange and antioxidant against 1, 1-diphenyl-2-picrylhydrazyl (DPPH) were studied. The Zeta-potential value of α -HNPs was conducted showing an increase from -44 to -66 mV, it assessed the good stability of the synthesized NPs. The high negative values of zeta-potential may be attributed to the polyphenolic constituents capping present in the extract which confirming their stabilization role for the synthesized NPs. Muthukumar and his co-authors recommended that the green α -HNPs could be used effectively in environmental applications and also to address future biomedical concerns.

Jitendra and his co-authors [130] also in 2015 published their paper entitled " α - Fe_2O_3 hexagonal cones synthesized from the leaf extract of *Azadirachta indica* and its thermal catalytic activity". At room temperature, α -HNPs were bio-synthesized in a short reaction time of about two minutes, and the reaction solution was changed instantly to assure that NPs formation. UV-Vis spectrum showed an absorption peak around 565 nm, indicating the formation of α -HNPs, and the energy band gap was calculated and found to be 2.19 eV which found quite high when compared to the bulk α - Fe_2O_3 indication that NPs formation according to decreasing in the particles size. Thermal stability also was evaluated using TGA-DSC analysis manifesting on the stability up to $600\text{ }^\circ\text{C}$ with residual content of about 79 % of pure α -HNPs. The average crystallite size from the XRD data was found to be around 38.2 nm and the crystal system found to be matched the corresponding rhombohedral phase of α -HNPs with crystalline nature. Hexagonal cone-like morphology was revealed using FESEM analysis with an average diameter of 400–500 nm. HRTEM revealed that the lattice spacing equals 0.525 nm which was in excellent agreement with the lattice spacing of rhombohedral Hematite. Jitendra et al. reported that the green synthesized α -HNPs can be used as an efficient catalyst for enhancing the thermal decomposition of ammonium perchlorate and the combustion of composite solid propellants.

In 2016, a biogenic synthesis of α -HNPs was conducted by Alex et al. [32] using the extract of *Guava* (*Psidium guajava*) leaves. They reported that the as-phyto-synthesized α -HNPs was in crystalline in nature, high purity with a rhombohedral crystallographic system which demonstrated using XRD with average crystallite size 34.1 nm. UV-Vis-NIR absorption spectrometric analysis revealed four absorption peaks at wavelengths 347 nm, 543 nm, 652 nm, and 849 nm. The PL spectrum showed an emission peak at 688 nm when the α -HNPs was excited at 460 nm. The direct & indirect band gaps were be estimated and found to be 1.71 eV and 1.56 eV respectively. The VSM study was conducted and revealed that the observed M_s of the synthesized sample was 0.3152 emu/g. A quasi-spherical shape morphology was illustrated using SEM analysis. The antibacterial efficacy against *E. coli* and *S. aureus* pathogens were

conducted and revealed a high antibacterial activity for the as- Phyto synthesized α -HNPs.

In 2016 also, a greener and eco-friendly one-pot method for synthesizing α -HNPs using ultrasonic irradiation of iron (III) oxide solution containing the aqueous root extract of *Arisaema amurense* was reported by Kannan and Sung [2]. They used many and different techniques for the characterization of the as-fabricated NPs. UV-Vis absorption spectrum manifested a peak at 570 nm indicating the formation of α -HNPs. FT-IR results indicated the presence of stabilizing groups on the surfaces of the formed NPs. The purity of α -HNPs was assured using XRD analysis showing an average crystallite size of about 23.98 nm using the Scherrer equation. TEM outcomes revealed that the formed α -HNPs near-spherical with an average size of 24.55 ± 6.9 nm. SEM showed slightly agglomerated NPs sized about 100 nm. The thermal analysis also has been checked using TGA showing thermal stability of 30 % from the initial mass up to $990\text{ }^\circ\text{C}$ approximately. At room temperature, VSM analysis confirmed the ferromagnetic nature of the α -HNPs with M_s at 1.25 emu/g. Cyclic voltammetry study results explored the electrochemical behavior of the as-fabricated NPs. Zeta potential results manifested moderate stability at -23.3 ± 6.83 mV value. Cytotoxicity to human keratinocytes CRL-2310 was conducted indicating that IC_{50} for the synthesized α -HNPs equal 800 $\mu\text{g}/\text{mL}$.

Hager and her co-workers [98] in 2017 issued their paper entitled "Green synthesis of α - Fe_2O_3 using *Citrus reticulatum* peels extract and water decontamination from different organic pollutants", Mandarin peels "*Citrus reticulatum*" consider as a way for the recycling of domestic waste into a valuable product. The as-formation of α -HNPs was depicted using a UV-Vis spectrophotometer where an appearance of the broad peak in the range 318–608 nm with maximum absorbance at 384 nm; the energy band gap was calculated and found to be 2.38 eV. Thermal profile and stability were conducted using TGA revealed mass constant beyond 650 – $800\text{ }^\circ\text{C}$. FT-IR analysis assured capping process with organic constituents that appeared in the α -HNPs spectrum. The resultant data of XRD were found to be identical with the pure crystalline α -HNPs rhombohedral pattern after annealing up to $800\text{ }^\circ\text{C}$. The average crystallite size for the as-prepared α -HNPs was calculated and found to be about 57.59 nm using Debye-Scherrer's equation. SEM analysis of the calcined α -HNPs demonstrated that porous sphere-shaped particles with rough surfaces; where TEM revealed the aggregates of porous, irregular, rough, and quasi-spherical shaped particles with particles size between 20 and 63 nm which approximately agreed with that calculated of XRD. VSM analysis recorded that $M_s = 2.4168$ emu/g which revealed weak ferromagnetic behavior. The photocatalytic activity was explored under visible light irradiation against different organic pollutants indicating that the conclusive ability of the phyto fabricated α -HNPs as a superior catalyst.

In 2017 Silvia et al. [34] conducted the synthesis of α -HNPs using *Cynometra ramiflora* extract. SEM images showed discrete spherical shaped particles. The XRD results depicted the crystalline structure of α -HNPs. FT-IR spectra portrayed the existence of functional groups of phytochemicals which are probably involved in the formation and stabilization of NPs, the synthesis of α -HNPs was confirmed where the bands less than 800 cm^{-1} corresponds to the vibration of Fe–O bonds. The α -HNPs exhibited effective inhibition against *E. coli* and *S. epidermidis* assuring its antibacterial role in drug development. Furthermore, the catalytic activity of the α -HNPs as a Fenton-like catalyst was successfully investigated for the degradation of Rhodamine-B dye; so, this outcome could play a prominent role in the wastewater treatment.

As well in 2017 Rajiv et al. [36] selected the green route for the synthesis of the α -HNPs using *Lantana camara* leaf extract. In this study, the UV-Vis absorption spectrum revealed a wide absorption peak at 370 nm. In their investigation, FT-IR was conducted to confirm that the biomolecules that present on the shell of bio-synthesized α -HNPs corresponding to that present in the plant extract to prove the capping process. XRD analysis also was performed, the obtained peaks were broad with particle size between 10–20 nm. They evaluated the biological activities

for the as-prepared α -HNPs *P. aeruginosa* at a concentration of 100 $\mu\text{g}/\text{mL}$. Assessing the effect of the as-prepared α -HNPs on seed germination, shoot and root development in *Vigna mungo* was conducted; the highest percentage of seeds was germinated (87 %) at 200 ppm concentration of synthesized α -HNPs.

α -HNPs were successfully synthesized using *Cyperus rotundus* L. by Nagaraj et al. [50] in 2017. They reported that the phyto-synthesized α -HNPs were highly crystalline with a face-centered cubic system without the presence of any impurities which was illustrated using XRD analysis. FT-IR analysis also was conducted to assure that the obtained α -HNPs were stabilized by bioactive constituents in *Cyperus rotundus* L., TGA outcome revealed that the biosynthesized α -HNPs were thermally stable up to 700 °C. The morphology of the surface was examined by SEM analysis showing slightly irregular in shape and size, the porous structure formed by the network of spherical NPs interlinked over a rhombohedral material. The TEM images of the α -HNPs showed that the particles were monodispersed with few agglomerates in both spherical and rhombohedral nature; also, the mean grain size was found to be approximately 60–80 nm. VSM test at room temperature was implemented to understand the magnetic behavior of the biosynthesized α -HNPs; $M_s = 10.01$ emu/g in a linear relationship between the applied magnetic field and magnetization measurements up to 5000 Oe revealing the ferromagnetic for the formed NPs. The as-synthesized α -HNPs exhibited strong catalytic activity for the reduction of 4-nitro-o-phenylenediamine to 1,2,4-benzotriamine in the presence of NaBH_4 and the degradation of Congo red dye by the photocatalytic method. The biosynthesized α -HNPs revealed a high ability to be recovery and reusability in the same reduction reaction under identical conditions up to three times without any significant loss.

In 2018, in another similar experiment using a different part of the *Cynometra ramiflora* plant; the fruit extract waste was introduced by Shahana et al. [131] to synthesize a mixture of α -HNPs & β -HNPs. By performing the FT-IR identification test and comparing the phytochemicals present in the *Cynometra ramiflora* fruit and those observed in the NPs chart, the reduction process, and capping role were be ascertained. Based on the XRD data, the as-synthesized material displayed a high purity, the crystalline, rhombohedral structure of the α -HNPs phase. Also, a much smaller peak was be observed corresponds to $\beta\text{-Fe}_2\text{O}_3$. The crystallite size was evaluated by the Debye-Scherrer equation and it was found to be 68.17 nm. According to the BET analysis; the surface area of the prepared NPs was determined and found to be 107.97 m^2/g while the surface area of the commercial Hematite is just 7.7 m^2/g ; on the other hand, the surface area of α -HNPs which chemically prepared was found to be 18.8 m^2/g . Also, the zero-point charge was estimated for the as-prepared α -HNPs and found to be 8.1 consistent was consistent with the previously reported value. Photocatalytic activity under sunlight irradiation was explored using the as-synthesized α -HNPs as a catalyst against methylene blue dye pollutant aqueous solution degradation and high performance was achieved to get rid of the organic contaminant.

In another study in the same 2018, Low-cost α -HNPs were successfully synthesized using *Ailanthus excelsa* leaves by Hassan et al. [109]. The formation of α -HNPs was confirmed using XRD; it was revealed in crystal phase pure crystalline monoclinic structure with average crystallite size 40 nm. The potential engagement of polyphenols, flavonoids, and other predicted biomolecules in the synthesized NPs was recognized under the FT-IR test. Stability and formation of the as-prepared α -HNPs in sterile distilled water were conducted using UV-Vis spectroscopy; the spectrum showed an absorption peak at 450 nm dedicated to α -HNPs. Morphology nature characterized using SEM analysis; where a spherical within diameters range 5–200 nm. The as-biosynthesized α -HNPs were conducted as an insecticidal agent and it manifested an admirable efficacy on the mortality of green peach aphid at $\text{LC}_{50} = 1125$ ppm. Also, the Phytotoxicity effect on the treated pepper leaves was observed at high concentrations.

Moringa oleifera leaf extract was explored in 2018 as a greener method for the phytofabrication of α -HNPs by Silveira et al. [132]. Diffractograms obtained by XRD assured the amorphous nature of the

synthesized α -HNPs in a rhombohedral crystallographic system with a 7 nm average diameter estimated by the Scherrer equation. SEM morphology was illustrated as an agglomerated spherical particle of α -HNPs. The particles with an average diameter of less than 100 nm of α -HNPs forming darker coloration agglomerates were be shown using TEM analysis. The biosynthesized α -HNPs revealed favorable adsorption of fluoride ions in 40 min with maximum adsorption capacity 1.4 mg/g at pH 7; the isotherm model was found to be fit for the Langmuir model; the best described kinetic data was found to be pseudo-first-order. Additionally, the thermodynamic parameters indicated spontaneous and endothermic adsorption reaction; the regeneration process showed that is possible to reuse α -HNPs three times in the fluoride ions adsorption process.

2019 is the most prolific and densities year in the scientific outcome, with nearly eight studies submitted and completed compared to an average of two or three published studies in each year over the past five years in α -HNPs biosynthesis. Also, new types of applications and activities that witnessed a wide variety of different purposes were exposed by using as-biosynthesized α -HNPs using the plant extracts by green chemistry. The unique properties of the bio-fabricated NPs by this pathway technology "biosynthesis using plant extracts" were favored used for being easy, simple, cost-effective, non-toxic, and eco-friendly.

Recently in 2019, Ismat [133] and his co-workers introduced a green synthesis of α -HNPs using pomegranate (*Punica granatum*) seeds extract for the first time. The LCMS/MS was performed to identification of biomolecule present in the extract of pomegranate seeds, *p*-hydroxybenzoic acid, gallic acid, methyl gallate, catechin, kaempferol-3-*O*-sophoroside, 3-deoxyflavonoids, magnolol, ferulic acid, vanillic acid, and pinoembrin along with other minor constituents were detected in the extracts using for the synthesis of IONPs. The average grain size was 48 nm using XRD analysis. The adopted green route furnished semi-spherical uniformly distributed of the particles. SEM analysis and the particle size were found in the range of 25–55 nm. The absorption spectrum of the as-prepared α -HNPs was revealed an absorption peak at 371.71 nm. The photocatalytic activity was conducted for blue 4 dye using HPLC for the following up the degradation profile of the dye under UV light irradiation. 95.08 % of dye degradation was achieved within 56 min.

A facile biosynthesis of α -HNPs was reported in 2019 by Jegadeesan et al. [37] using aqueous extracts of three plant sources: *Terminalia bellirica*; *Moringa oleifera* fruit and *Moringa oleifera* leaves. The total phenolic content was performed and found to be the highest in *Terminalia bellirica* extract as gallic acid. α -HNPs showed absorption peaks at around 300 nm and 400 nm. FT-IR identification was conducted for assurance of the capping process of the as-synthesized NPs. SEM analysis was used for surface and shape description of the NPs which was found to be spherical in the case of *Terminalia bellirica* while irregularly shaped for the others. XRD analysis confirmed the formation of α -HNPs. The antioxidant activity of the aqueous extracts was achieved and it was found to be higher than that of the biogenic α -HNPs. The antimicrobial activity for *S. aureus*, *B. subtilis*, *P. aeruginosa*. also conducted against synthesized NPs. The antimicrobial activity for α -HNPs was higher than the extract alone.

Also, in 2019 the biogenic synthesis of α -HNPs via *Skimmia Laureola* leaf extract was conducted by Tariq et al. [38]. They reported that the synthesized α -HNPs were crystalline with cubic morphology which was illustrated using SEM analysis within the diameter range 56–350 nm. UV-Vis absorption spectrometric analysis revealed absorption spectra at a wavelength of 318 nm. FT-IR analysis also was conducted to assure that the obtained α -HNPs were capped by biomolecules in *Skimmidiol*, and these metabolites may be responsible for the biogenic synthesis of α -HNPs. XRD data resulted that the average particle size of biogenic α -HNPs 34 ± 0.37 nm. The antibacterial efficacy against bacterial tomato wilt pathogen *R. solanacearum* in vitro and planta was conducted and revealed a strong antibacterial activity for the synthesized NPs.

In the same year 2019. Shraddha et al. [40], *Henna (Lawsonia inermis)* leaf extract "L-tyrosine -functionalized α -HNPs synthesis" has been

reported. L-tyrosine was used for capping and stabilizing the bio-synthesized IONPs. SEM analysis results demonstrated that the produced particles are spherical in the range of 150–200 nm. FT-IR results indicated the presence of the OH group in the produced α -HNPs. The characteristic peak was found to be around 220–224 nm using UV-Vis spectroscopy. The prepared α -HNPs in solution were kept at ambient conditions of light and periodically the absorption spectra of the NPs were conducted up to 30 days showing high stability. Antimicrobial activity was performed by L-tyrosine-functionalized α -HNPs against both *S. aureus* and *S. typhimurium* revealing great potential as an antimicrobial agent.

Green biosynthesis of α -HNPs was reported by Abusalem et al. in 2019 [41] using aqueous extracts of *Pistachio* leaf (*Pistacia vera* L) extract at ambient temperature. UV-Vis absorption spectrometric analysis revealed the surface plasmon resonance peak at a wavelength of 480 nm; this demonstrates the spherical shape of the α -HNPs which was confirmed after that by TEM images with a narrow-size distribution showing particle size 40 nm. FT-IR identification was conducted for assurance of the capping and stabilization process of the as-synthesized NPs. XRD analysis confirmed the formation of hexagonal crystalline α -HNPs with particle size 40 nm. Conduction of 10 ppm concentration of α -HNPs was found to be adequate to promote the seed vigor index of tomato seeds so, the α -HNPs biosynthesized NPs using this pathway in the fabrication can be utilized as a priming technique in agricultural production.

In 2019 also, a successfully greener and eco-friendly method for synthesizing α -HNPs entitled “Green synthesis of hematite (α -Fe₂O₃) NPs using *Rhus punjabensis* extract and their biomedical prospect in pathogenic diseases and cancer” was issued by Sania et al. [30]. They reported that the *Rhus Punjabensis* extract potential as both reducing and capping agents for phyto-mediated synthesis of NPs. The structure, morphology were carried out with different investigation tools. UV-Vis absorption spectrum manifested a peak at 283 nm indicating the formation of α -HNPs. Also, the energy band gap was calculated and found to be in a range of 1.85–1.90 eV. The crystallinity of as-prepared α -HNPs was assured using XRD analysis revealing a rhombohedral crystal system with an average crystallite size of about 35 nm using the Scherer equation. For identification, the role of bioactive molecules in the reduction and stabilizing of the NPs; FT-IR analysis was conducted. The thermal behavior profile of the as-prepared α -HNPs also has been studied using TGA where it was shown high thermal stability without any change with temperature increase up to 850 °C. SEM outcomes revealed that the formed α -HNPs near to spherical with narrow size distribution at low magnification, while it has appeared as polyhedral faceted in shape at high magnification. TEM showed an agreement with SEM results in average particle size which was found to be a rounded 48 nm and it was near the size calculated by the Scherer equation. The α -HNPs exhibited significant cytotoxic potential against the leishmanian parasite (amastigotes) with IC₅₀ 101 μ g/mL. The prepared α -HNPs also revealed a high antibacterial efficacy against each of Gram-positive bacteria “*S. aureus*” and Gram-negative bacteria “*P. aeruginosa*, *B. bronchiseptica* & *E. coli*”. Additionally, the as-prepared α -HNPs was found to be active against various cancer cell lines like (PC-3 & DU-145) for prostate cancer at IC₅₀ equal 45.2 μ g/mL & 12.79 μ g/mL respectively, (HL-60) human promyelocytic leukemia cells at IC₅₀ = 11.96 μ g/mL and (HT-29) at IC₅₀ = 5.82 μ g/mL.

As well in 2019, *Sida cordifolia* plant extract was used as an eco-friendly method aiming to synthesized α -HNPs in a successful trial by Panduranga et al. [97]. Methanolic extract of *Sida cordifolia* plant was used in HPTLC engaged with LC-MS/TOF analysis to investigate the actual composition which assured the presence of various phytoconstituents including, glycosides, carbohydrates, proteins, tannins, flavonoids, alkaloids, and terpenoids. Based on XRD data; a high purity of the rhombohedral α -HNPs was fabricated within about 18 nm crystallite size calculated via Debye-Scherrer. FT-IR analysis was performed to identify and confirm the adsorption and contribution of the organic bioactive molecules on the surface of the as-prepared NPs. According to the examined surface morphology using SEM analysis; an aggregation of the

as-prepared α -HNPs in a spherical nanocluster was manifested. TEM analysis has been implemented showing an asymmetric morphology with a uniform distribution for the as-synthesized α -HNPs with an average particle size of 16 nm which identical to the predicted result from XRD analysis with Debye-Scherrer. The thermogram profile revealed high stability of the formed α -HNPs up to 800 °C. The as-green synthesized α -HNPs showed an admirable efficacy in antibacterial activity especially as implemented against the microbial species in the current study either Gram-positive “*B. subtilis* & *S. aureus*” or Gram-negative “*E. coli* & *K. pneumonia*”.

Kalyaniet and Shampa as well in 2019 [45] explored the size-controlled superparamagnetic α -HNPs using the green route for synthesis using *Garlic* extract. In this study, the UV-Vis absorption spectrum revealed a wide absorption peak at 450 nm. In their investigation, FT-IR was conducted to confirm that the biomolecules that present on the shell of bio-synthesized α -HNPs corresponding to that present in the plant extract to prove the capping process. Additionally, the characteristic band of Fe–O at 587 cm⁻¹ was revealed. XRD analysis also was performed, the obtained particle size was calculated using the Scherer equation and found to be 8 nm corresponding hexagonal crystal system. Zeta potential value was recorded and found to be in -36.8 mV assuring the good stability of bio-synthesized NPs when zeta potential value lied above the critical value \pm 25 mV. SEM analysis also was conducted and revealed that the as-prepared α -HNPs were spherical with uniform distribution. Additionally, TEM analysis showed that the average particle size in the range of 20–30 nm. VSM was implemented to determine the magnetic properties of the α -HNPs at room temperature, the M_s was found 15.677 emu/g which indicating that superparamagnetic material was identified. TGA also was conducted exploring the high stability for the as-prepared α -HNPs up to 800 °C. The cytotoxic property for α -HNPs was analyzed against for cell lines of colorectal cancer (HCT 116), breast cancer (MCF-7), and cervical cancer (HeLa), and their IC₅₀ found to be 230 μ g/mL, 346 μ g/mL, and 285 μ g/mL respectively.

In the current year 2020, the biosynthesis of α -HNPs using *Rheum emodi* root with the green route was reported by Deepika et al. [46]. α -HNPs were synthesized in a cost-effective and eco-friendly method. The spherical shape and the average particle diameter of about 12 nm were conducted through TEM analysis. The morphology illustrated the homogeneity in grains with uniform distribution and revealed that α -HNPs dispersed completely without any traces of agglomeration in a smooth and spherical shape. FT-IR analysis revealed the presence of anthraquinone in *Rheum emodi* roots extract which plays the central role in the stabilization of the α -HNPs. The surface plasmon resonance peaks at 270 nm and 320 nm specified the synthesis of α -HNPs capped with hydroxy-anthraquinones was revealed using UV-Vis spectroscopy. XRD experiment assured the crystallinity nature of the synthesized NPs in the rhombohedral crystallographic system. The thermal property of *R. emodi* mediated α -HNPs was tested and elucidated the thermal stability up to 600 °C annealing. VSM exhibited a ferromagnetic behavior for the as-prepared NPs at room temperature at 4.07 emu/g. The α -HNPs showed good antibacterial activity against Gram-negative “*E. coli*” and Gram-positive “*S. aureus*” species additionally, it's a high ability for cervical cancer cell inhibition at 41.90 μ g/mL for IC₅₀.

Another paper issued by Abdolhossein et al. [43] in 2020 to biosynthesize the α -HNPs using the *Salvadora persica* aqueous extract. The results showed that the produced NPs are spherical in shape and uniform with particle size about 15–20 nm using SEM analysis. FT-IR technique was conducted for the confirmation capping process of the bio-synthesized NPs and the results indicated the presence of polyphenol groups in plants of aqueous extract which contributed to the reduction and stabilizing of the fabricated α -HNPs. The saturated magnetism M_s of the synthesized α -HNPs determined and found to be 1.8 emu/g which is higher than the commercial α -HNPs M_s = 0.6 emu/g. This result showed the superparamagnetic properties of the synthesized NPs. Cytotoxic activity of the biosynthesized α -HNPs was checked against colon (HT-29) cancer cell lines and the IC₅₀ was estimated and found to be 125 μ g/mL.

Table 4. Structural and morphological investigation of the biosynthesized α -HNPs.

Plant name/part	XRD Crystal system & particle size (nm)	SEM Shape & particle size (nm)	TEM Shape & particle size (nm)	Ref
<i>Arisaema amurense</i> root	Pure 23.98	Agglomerated NPs ~100	Spherical 24.55 ± 6.9	[2]
<i>Rhus punjabensis</i>	Crystalline & rhombohedral 35	Spherical/polyhedral faceted –	Spherical/polyhedral faceted 48	[30]
<i>Guava (Psidium guajava)</i> leaves	Pure, crystalline & rhombohedral 34.1	Quasi-spherical –	– –	[32]
<i>Cynometra ramiflora</i>	Crystalline –	Spherical –	– –	[34]
<i>Amaranthus dubius</i> leaf	Crystalline & rhombohedral –	Spherical 60–300	Spherical/cubic 43–220	[35]
<i>Lantana camara</i> leaf	– 10–20	– –	– –	[36]
<i>Terminalia bellirica</i> ; <i>Moringa oleifera</i> fruit & <i>Moringa oleifera</i> leaves	– –	Spherical for <i>Terminalia bellirica</i> & irregularly shaped for the others –	– –	[37]
<i>Skimmia Laureola</i> leaf	– 34 ± 0.37	Cubic 56–350	– –	[38]
<i>Henna (Lawsonia inermis)</i> leaf	– –	Spherical 150–200	– –	[40]
<i>Pistachio</i> leaf (<i>Pistacia vera</i> L)	Crystalline & hexagonal 40	– –	– 40	[41]
<i>Salvadora persica</i>	– –	Spherical 15–20	– –	[43]
<i>Hippuric acid</i> , <i>Itaconic acid</i> , <i>Tyrosine</i> <i>amino acid</i>	– 20–60	Spherical & hexagonal 5–50	Spherical 5–50	[44]
<i>Garlic extract</i>	Hexagonal 8	Spherical –	– 20–30	[45]
<i>Rheum emodi</i> root	Crystalline & rhombohedral –	Spherical –	Spherical 12	[46]
<i>Cyperus rotundus</i> L.	Pure, crystalline & face-center-cubic –	Irregular/porous/ spherical/rhombohedral	Spherical/rhombohedral 60–80	[50]
<i>Green Tea (Camellia sinensis)</i> leaves	Pure, crystalline & rhombohedral 33	– 40–80	Spherical & porous –	[66]
<i>Sida cordifolia</i>	Pure & rhombohedral 18	Spherical –	Asymmetric 10–22	[97]
<i>Mandarin peels “Citrus reticulatum”</i>	Pure, crystalline & rhombohedral 57.59	Porous/spherical/rough surfaces –	Aggregates porous/irregular/ rough & quasi-spherical 20–63	[98]
<i>Ailanthus excelsa</i> leaves	Pure, crystalline & monoclinic 40	Spherical 5–200	– –	[109]
<i>Curcuma</i>	Pure, crystalline & rhombohedral 4	– –	Spherical –	[128]
<i>Tea leaves</i>	Pure, crystalline & rhombohedral 5	– –	Spherical –	[128]
<i>Green Tea leaf</i>	Crystalline 28.9	Rods –	Rods Length = 130–150 & Width = 20	[129]
<i>Azadirachta indica</i> leaf	Crystalline & rhombohedral 38.2	Hexagonal cone 400–500	– –	[130]
<i>Cynometra ramiflora</i> fruit	Pure, crystalline & rhombohedral 68.17	– –	– –	[131]
<i>Moringa oleifera</i> leaf	Amorphous & rhombohedral 7	Spherical –	Darker coloration agglomerates <100	[132]
<i>Pomegranate (Punica granatum)</i> seeds	– 48	Semi-spherical 25–55	– –	[133]
<i>Laurus nobilis</i> L.	Pure, crystalline & rhombohedral 21.5	Semi-spherical 22.11–39.51	Spherical like/partly hexagonal 8.03 ± 8.99	[134]
<i>Cornus mas</i> L.	Pure, crystalline & rhombohedral 20	Spherical and spongy –	Very fine spherical 20–40	[135]

As well in 2020, the *Laurus nobilis* L. leaves aqueous extract was used as an eco-friendly method aiming to synthesized α -HNPs in a successful trial by Jamzad and Kamari [134]. The surface plasmon resonance peak at 285 nm was detected as biosynthesized of α -HNPs using UV-Vis spectroscopy. Based on XRD data; a high purity crystalline of a hexagonal rhombohedral α -HNPs was fabricated within about 21.5 nm crystallite

size calculated via Debye-Scherrer. FT-IR analysis was performed to identify and confirm the capping and contribution of the organic bioactive molecules on the surface of the as-prepared NPs. According to the examined surface morphology using SEM analysis; an aggregation of the as-prepared α -HNPs in a semi-spherical NPs was manifested in the ranges 22.11–39.51 nm. TEM analysis has been implemented showing a

Table 5. The Uv-vis absorption spectroscopic analysis and calculated/expected of the energy band gap for the biosynthesized α -HNPs.

Plant name/part	Uv-vis (nm)	Calculated E _g (eV)	Expected E _g (eV)	Ref
<i>Arisaema amurense</i> root	570	–	2.18	[2]
<i>Rhus punjabensis</i>	283	1.85–1.90	4.38	[30]
Guava (<i>Psidium guajava</i>) leaves	347, 543, 652 & 849	1.56–1.71	1.46–3.57	[32]
<i>Amaranthus dubius</i> leaf	214 at pH 4 300 at pH 9	–	5.79 at pH 4 4.13 at pH 4	[35]
<i>Lantana camara</i> leaf	370	–	3.35	[36]
<i>Terminalia bellirica</i> ; <i>Moringa oleifera</i> fruit & <i>Moringa oleifera</i> leaves	300 & 400	–	3.10–4.13	[37]
<i>Skimmia Laureola</i> leaf	318	–	3.90	[38]
Henna (<i>Lawsonia inermis</i>) leaf	220–224	–	5.54–5.64	[40]
Pistachio leaf (<i>Pistacia vera</i> L)	480	–	2.58	[41]
Garlic extract	450	–	2.76	[45]
<i>Rheum emodi</i> root	270 & 320	–	3.88–4.59	[46]
Green Tea (<i>Camellia sinensis</i>) leaves	290–310 & 485–550	–	2.25–4.28	[66]
Mandarin peels “ <i>Citrus reticulatum</i> ”	384	2.38	3.23	[98]
<i>Ailanthus excelsa</i> leaves	450	–	2.76	[109]
<i>Curcuma</i>	561, 442 & 272	2.2	2.21–4.56	[128]
Tea leaves	551, 430 & 272	2.25	2.25–4.56	[128]
<i>Azadirachta indica</i> leaf	565	2.19	2.19	[130]
Pomegranate (<i>Punica granatum</i>) seeds	371.71	–	3.34	[133]
<i>Laurus nobilis</i> L.	285	–	4.35	[134]

Table 6. The thermal stability and magnetic property of the biosynthesized α -HNPs.

Plant name/part	TGA (C)	Ms (emu/g)	Ref
<i>Arisaema amurense</i> root	990	1.25	[2]
<i>Rhus punjabensis</i>	850	–	[30]
Guava (<i>Psidium guajava</i>) leaves	–	0.3152	[32]
<i>Salvadora persica</i>	–	1.8	[43]
Garlic extract	800	15.677	[45]
<i>Rheum emodi</i> root	600	4.07	[46]
<i>Cyperus rotundus</i> L.	700	10.01	[50]
Green Tea (<i>Camellia sinensis</i>) leaves	700	–	[66]
<i>Sida cordifolia</i>	800	–	[97]
Mandarin peels “ <i>Citrus reticulatum</i> ”	800	2.4168	[98]
<i>Azadirachta indica</i> leaf	600	–	[130]

spherical-like and hexagonal shape in a uniform distribution for the as-synthesized α -HNPs with an average particle size of 8.03 ± 8.99 nm which shows a difference about the resultant from XRD analysis with Debye-Scherrer which may be attributed to the wide range size distribution of the NPs. The as-green synthesized α -HNPs showed moderate efficacy in antimicrobial activity as implemented against the microbial species in the current study either Gram-positive bacterium of *Listeria monocytogenes* or two fungi; *Penicillium spinulosum* and *Aspergillus flavus*.

Also, in 2020 the biogenic synthesis of α -HNPs via fruit extract of *Cornus mas* L. was conducted by Rostamizadeh et al. [135]. They reported that the biosynthesized α -HNPs were pure crystalline in nature with rhombohedral morphology at an average particle size of 20 nm based on XRD data analysis. SEM analysis illustrated shapes as spherical and spongy particles. FT-IR analysis also was conducted to assure that the obtained α -HNPs were capped by biomolecules in *Cornus mas* L. extract,

Table 7. The surface zeta potential property of the biosynthesized α -HNPs.

Plant name/part	Zeta potential (mV)	Ref
<i>Arisaema amurense</i> root	-23.3 \pm 6.83	[2]
<i>Amaranthus dubius</i> leaf	-44 to -66	[35]
Garlic extract	-36.8	[45]

and these metabolites may be responsible for the biogenic synthesis of α -HNPs. The TEM result showed very fine spherical NPs in the range 20–40 nm which are very close to XRD calculations. The biosynthesized NPs showed improved growth of barley seedlings relative to the corresponding levels of bulk counterparts.

Tables 4, 5, 6, 7, and 8 summarized the different plant extracts used for α -HNPs biosynthesis, characterization, physicochemical properties, and potential applications.

4. Limitations of the green approach via plant extracts for the biosynthesis of nanomaterials

The limitations of this method located where; in some cases, we have to use a high concentration of the plant extract that contains a low concentration of the bioactive molecules; in another word the selected plant does not have enough content of the bioconstituents that work as a reducing, capping and stabilizing agent at the same time. So, we have to modify the reaction conditions like pH, temperature, time, and sometimes the reaction should be conducted under nitrogen gas to prevent the formation of the undesirable oxides nanomaterials. Besides, we can't predict the type of resultant nanomaterial at first till we make a suitable and convenient characterization technique for investigation and identification.

Table 8. The different applications of the biosynthesized α -HNPs.

Plant name/part	Application	Ref
<i>Arisaema amurense</i> root	Cytotoxicity "Human keratinocytes CRL-2310 at IC ₅₀ = 800 μ g/mL"	[2]
<i>Rhus punjabensis</i>	Cytotoxic "Leishmanial parasite (amastigotes) with IC ₅₀ 101 μ g/mL" Antibacterial activity "S. aureus, P. aeruginosa, B. bronchiseptica & E. coli" Anticancer activity "Cell lines (PC-3 & DU-145) for prostate cancer at IC ₅₀ = 45.2 μ g/mL & 12.79 μ g/mL respectively, (HL-60) human promyelocytic leukemia cells at IC ₅₀ = 11.96 μ g/mL & (HT-29) at IC ₅₀ = 5.82 μ g/mL"	[30]
Guava (<i>Psidium guajava</i>) leaves	Antibacterial activity "E. coli & S. aureus"	[32]
<i>Cynometra ramiflora</i>	Antibacterial activity "E. coli & S. epidermidis" Photocatalytic activity "Rhodamine-B dye degradation"	[34]
<i>Amaranthus dubius</i> leaf	Photocatalytic degradation "Methylene orange dye" Antioxidant "1, 1-diphenyl-2-picrylhydrazyl (DPPH)"	[35]
<i>Lantana camara</i> leaf	Antibacterial activity "P. aeruginosa" Agriculture "Seed germination, shoot and root in <i>Vigna mungo</i> at 200 ppm"	[36]
<i>Terminalia bellirica</i> ; <i>Moringa oleifera</i> fruit & <i>Moringa oleifera</i> leaves	Antibacterial activity "S. aureus, B. subtilis & P. aeruginosa"	[37]
<i>Skimmia Laureola</i> leaf	Antibacterial activity "R. solanacearum"	[38]
<i>Henna (Lawsonia inermis)</i> leaf	Antibacterial activity "S. aureus & S. typhimurium"	[40]
<i>Pistachio</i> leaf (<i>Pistacia vera</i> L)	Agricultural production "It promotes the seed vigor index of tomato seeds"	[41]
<i>Salvadora persica</i>	Anticancer activity "Colon (HT-29) cancer cell lines at IC ₅₀ = 125 μ g/mL"	[43]
Hippuric acid, Itaconic acid, Tyrosine amino acid	Anticancer "Breast carcinoma cells (MCF-7 cell line) IC ₅₀ at 3.10–3.81 μ g/mL"	[44]
Garlic extract	Anticancer activity "Colorectal cancer (HCT 116), breast cancer (MCF-7) & cervical cancer (HeLa) at IC ₅₀ found to be 230 μ g/mL, 346 μ g/mL and 285 μ g/mL respectively"	[45]
<i>Rheum emodi</i> root	Antibacterial activity "E. coli and S. aureus" Anticancer activity "Cervical cell at IC ₅₀ = 41.90 μ g/mL"	[46]
<i>Cyperus rotundus</i> L.	Catalytic activity "Reduction of 4-nitro-o-phenylenediamine" Photocatalytic activity "Congo red dye"	[50]
Green Tea (<i>Camellia sinensis</i>) leaves	Solar cells	[66]
<i>Sida cordifolia</i>	Antibacterial activity "B. subtilis & S. aureus, E. coli & K. pneumonia"	[97]
Mandarin peels " <i>Citrus reticulum</i> "	Photocatalytic activity	[98]
<i>Ailanthus excelsa</i> leaves	Insecticidal agent "Green peach aphid at LC ₅₀ = 1125 ppm"	[109]
<i>Curcuma</i>	Photocatalytic activity "Methyl orange dye"	[128]
Tea leaves	Photocatalytic activity "Methyl orange dye"	[128]
<i>Azadirachta indica</i> leaf	Thermal decomposition "Ammonium perchlorate enhancement"	[130]
<i>Cynometra ramiflora</i> fruit	Photocatalytic activity "Methylene blue dye"	[131]
<i>Moringa oleifera</i> leaf	Adsorption "Fluoride ions at maximum adsorption capacity 1.4 mg/g"	[132]
<i>Pomegranate (Punica granatum)</i> seeds	Photocatalytic activity "Blue 4 dye"	[133]
<i>Laurus nobilis</i> L.	Antibacterial activity as Gram-positive " <i>L. monocytogenes</i> " Antifungal activity as " <i>P. spinulosum</i> and <i>A. flavus</i> "	[134]
<i>Cornus mas</i> L.	Growth-promoting role in Barley	[135]

5. Conclusion

Since the dissemination and implementation of these concepts, α -HNPs green synthetic approaches have gained significant attention as they have offered revolutionary alternatives to physical and chemical synthetic routes by employing cost-effective, environmentally sustainable, and scalable techniques in the absence of either high-energy or hazardous chemical by-products. The variety of bioactive components of the different plant extracts encapsulating the NPs that have formed has contributed to the emergence of various properties, especially in the stability of these particles that have manifested in biological applications and as detection sensors. This review of the green biosynthesis of α -HNPs can provide a set of information on the phyto-fabrication with different characterization techniques of these NPs for their elevated potential use. In future prospects in this area, the various use of the plants can contribute in discover new physicochemical properties for the same nano-material that biosynthesized using different plant extracts. This progress enables us to discover many new applications to keep pace with the rapid development that we are living in especially in the next years.

Declarations

Author contribution statement

All authors listed have significantly contributed to the development and the writing of this article.

Funding statement

This research did not receive any specific grant from funding agencies in the public, commercial, or not-for-profit sectors.

Data availability statement

Data included in article/supplementary material/referenced in article.

Declaration of interests statement

The authors declare no conflict of interest.

Additional information

No additional information is available for this paper.

Acknowledgements

The corresponding author gratefully acknowledges the Academy of Scientific Research & Technology (ASRT), Egypt, Grant No. 6371 under the project Science Up., UP pharma industrial, Al-Esraa pharmaceutical optima industrial, Bio-Med industrial, and Smart pharma for pharmaceuticals for their valuable supports.

References

- [1] M. Arakha, et al., Antimicrobial activity of iron oxide nanoparticle upon modulation of nanoparticle-bacteria interface, *Sci. Rep.* 5 (2015) 14813.
- [2] K.B. Narayanan, S.S. Han, One-pot green synthesis of Hematite (α -Fe₂O₃) nanoparticles by ultrasonic irradiation and their in vitro cytotoxicity on human keratinocytes CRL-2310, *J. Cluster Sci.* 27 (5) (2016) 1763–1775.
- [3] Y. Chen, C. Lin, Effect of nano-hematite morphology on photocatalytic activity, *Phys. Chem. Miner.* 41 (10) (2014) 727–736.
- [4] D. Ramimoghadam, S. Bagheri, S.B.A. Hamid, Progress in electrochemical synthesis of magnetic iron oxide nanoparticles, *J. Magn. Magn. Mater.* 368 (2014) 207–229.
- [5] R.M. Cornell, U. Schwertmann, *The Iron Oxides: Structure, Properties, Reactions, Occurrences and Uses*, John Wiley & Sons, 2003.
- [6] A. Lassoued, et al., Synthesis, photoluminescence and Magnetic properties of iron oxide (α -Fe₂O₃) nanoparticles through precipitation or hydrothermal methods, *Phys. E Low-dimens. Syst. Nanostruct.* 101 (2018) 212–219.
- [7] S. Khorshidian, *Vibrating Sample Magnetometer and Hysteresis Loop*, Vol. 1, Yasouj University, 2019, pp. 1–36.
- [8] T. Štěpka, *Noninvasive Control of Magnetic State in Ferromagnetic Nanodots by Hall Probe Magnetometry*, Vol. 1, Slovak University, 2016, pp. 1–123.
- [9] C. Chen, *Magnetism and Metallurgy of Soft Magnetic Materials*, *Dover Pub. Inc.*, New York, 1986.
- [10] A.K. Gupta, M. Gupta, Synthesis and surface engineering of iron oxide nanoparticles for biomedical applications, *Biomaterials* 26 (18) (2005) 3995–4021.
- [11] S. Elliott, *The Physics and Chemistry of Solids*, Wiley, 1998.
- [12] T. Sato, et al., Magnetic properties of ultrafine ferrite particles, *J. Magn. Magn. Mater.* 65 (2–3) (1987) 252–256.
- [13] J. Dormann, E. Tronc, D. Fiorani, *Advances in Chemical Physics Series Vol. 98*, Wiley, New York, 1997, p. 283.
- [14] S. Lefebure, et al., Monodisperse magnetic nanoparticles: preparation and dispersion in water and oils, *J. Mater. Res.* 13 (10) (1998) 2975–2981.
- [15] C. Bean, u.D. Livingston, Superparamagnetism, *J. Appl. Phys.* 30 (4) (1959) S120–S129.
- [16] J. Chatterjee, Y. Haik, C.-J. Chen, Size dependent magnetic properties of iron oxide nanoparticles, *J. Magn. Magn. Mater.* 257 (1) (2003) 113–118.
- [17] Y. Li, et al., Hall magnetometry on a single iron nanoparticle, *Appl. Phys. Lett.* 80 (24) (2002) 4644–4646.
- [18] D. Han, J. Wang, H. Luo, Crystallite size effect on saturation magnetization of fine ferrimagnetic particles, *J. Magn. Magn. Mater.* 136 (1–2) (1994) 176–182.
- [19] F. Tourinho, et al., Synthesis and magnetic properties of manganese and cobalt ferrofluids, *Prog. Colloid Polym. Sci.* 79 (1989) 128–134.
- [20] S. Gomez-Lopera, R. Plaza, A. Delgado, Synthesis and characterization of spherical magnetite/biodegradable polymer composite particles, *J. Colloid Interface Sci.* 240 (1) (2001) 40–47.
- [21] W. Voit, et al., Magnetic behavior of coated superparamagnetic iron oxide nanoparticles in ferrofluids, *Mater. Res. Soc. Symp. Proc.* 676 (2001) 1–6.
- [22] A. Bradbury, et al., Magnetic size determination for interacting fine particle systems, *IEEE Trans. Magn.* 20 (5) (1984) 1846–1848.
- [23] G. Sharma, P. Jeevanandam, Synthesis of self-assembled prismatic iron oxide nanoparticles by a novel thermal decomposition route, *RSC Adv.* 3 (1) (2013) 189–200.
- [24] W. Wu, et al., Large-scale and controlled synthesis of iron oxide magnetic short nanotubes: shape evolution, growth mechanism, and magnetic properties, *J. Phys. Chem. C* 114 (39) (2010) 16092–16103.
- [25] Z. Zhang, C. Boxall, G. Kelsall, Photoelectrophoresis of colloidal iron oxides 1. Hematite (α -Fe₂O₃), in: *Colloids in the Aquatic Environment*, Elsevier, 1993, pp. 145–163.
- [26] L. Macera, et al., Nano-sized Fe (III) oxide particles starting from an innovative and eco-friendly synthesis method, *Nanomaterials* 10 (2) (2020) 323.
- [27] H.M. Al-Saidi, G.A. Gouda, O. Farghaly, Potentiometric study of a new Schiff base and its metal ion complexes: preparation, characterization and biological activity, *Int. J. Electrochem. Sci.* 15 (2020) 10785–10801.
- [28] A.M.A. Aly, et al., Thermal stability of Ni (II) and Cu (II) mixed ligand complexes derived from biologically important Schiff bases, Azoles and morpholine, *Bull. Pharmaceut. Sci. Assiut* 31 (1) (2008) 93–108.
- [29] A.M.A. Aly, et al., Reactivity of certain biologically important Azoles and morpholine towards Ni (II) and Cu (II) complexes of o-hydroxyacetophenoneethanolimine and N-Salicylidene derivatives, *Bull. Pharmaceut. Sci. Assiut* 29 (1) (2006) 134–149.
- [30] S. Naz, et al., Green synthesis of hematite (α -Fe₂O₃) nanoparticles using *Rhus punjabensis* extract and their biomedical prospect in pathogenic diseases and cancer, *J. Mol. Struct.* 1185 (2019) 1–7.
- [31] M. Bhushan, et al., Synthesis of α -Fe₂O₃ nanocrystals and study of their optical, magnetic and antibacterial properties, *RSC Adv.* 5 (40) (2015) 32006–32014.
- [32] A. Rufus, N. Sreeju, D. Phillip, Synthesis of biogenic hematite (α -Fe₂O₃) nanoparticles for antibacterial and nanofluid applications, *RSC Adv.* 6 (96) (2016) 94206–94217.
- [33] P. Rajiv, et al., Degradation of bromothymol blue by 'greener' nano-scale zero-valent iron synthesized using tea polyphenols, *J. Mater. Chem.* 19 (45) (2009) 8671–8677.
- [34] S. Groiss, et al., Structural characterization, antibacterial and catalytic effect of iron oxide nanoparticles synthesized using the leaf extract of *Cynometra ramiflora*, *J. Mol. Struct.* 1128 (2017) 572–578.
- [35] M. Harshiny, C.N. Iswarya, M. Matheswaran, Biogenic synthesis of iron nanoparticles using *Amaranthus dubius* leaf extract as a reducing agent, *Powder Technol.* 286 (2015) 744–749.
- [36] P. Rajiv, et al., Synthesis and characterization of biogenic iron oxide nanoparticles using green chemistry approach and evaluating their biological activities, *Biocatal. Agric. Biotechnol.* 12 (2017) 45–49.
- [37] G.B. Jegadeesan, et al., Green synthesis of iron oxide nanoparticles using *Terminalia bellirica* and *Moringa oleifera* fruit and leaf extracts: antioxidant, antibacterial and thermoacoustic properties, *Biocatal. Agric. Biotechnol.* 21 (2019) 101354.
- [38] T. Alam, et al., Biogenic synthesis of iron oxide nanoparticles via *Skimmia laureola* and their antibacterial efficacy against bacterial wilt pathogen *Ralstonia solanacearum*, *Mater. Sci. Eng. C* 98 (2019) 101–108.
- [39] T. Alam, et al., Biosynthesis of iron oxide nanoparticles via *crocus sativus* and their antifungal efficacy against verticillium wilt pathogen *verticillium dahliae*, *BioRxiv* (2019) 861401.
- [40] S. Chauhan, L.S.B. Upadhyay, Biosynthesis of iron oxide nanoparticles using plant derivatives of *Lawsonia inermis* (Henna) and its surface modification for biomedical application, *Nanotechnol. Environ. Eng.* 4 (1) (2019) 8.
- [41] M. Abusaleem, et al., Green synthesis of α -Fe₂O₃ nanoparticles using Pistachio leaf extract influenced seed germination and seedling growth of tomatoes, *Jordan J. Earth Environ. Sci.* 10 (3) (2019) 161–166.
- [42] S.D. Brown, et al., Gold nanoparticles for the improved anticancer drug delivery of the active component of oxaliplatin, *J. Am. Chem. Soc.* 132 (13) (2010) 4678–4684.
- [43] A. Miri, M. Khatami, M. Sarani, Biosynthesis, magnetic and cytotoxic studies of hematite nanoparticles, *J. Inorg. Organomet. Polym. Mater.* 30 (3) (2020) 767–774.
- [44] A.H. Atta, et al., Synthesis and spectroscopic investigations of iron oxide nanoparticles for biomedical applications in the treatment of cancer cells, *J. Mol. Struct.* 1086 (2015) 246–254.
- [45] K. Rath, S. Sen, Garlic extract based preparation of size controlled superparamagnetic hematite nanoparticles and their cytotoxic applications, *Indian J. Biotechnol.* 18 (2019) 108–118.
- [46] D. Sharma, et al., Biosynthesis of hematite nanoparticles using *Rheum emodi* and their antimicrobial and anticancerous effects in vitro, *J. Photochem. Photobiol. B Biol.* (2020) 111841.
- [47] M.S. Saddik, et al., Biosynthesis, characterization, and wound-healing activity of phenytoin-loaded copper nanoparticles, *AAPS PharmSciTech* 21 (5) (2020) 1–12.
- [48] D.Z. Husein, R. Hassanien, M.F. Al-Hakkani, Green-synthesized copper nano-adsorbent for the removal of pharmaceutical pollutants from real wastewater samples, *Heliyon* 5 (8) (2019) e02339.
- [49] S. Sarkar, et al., Hybrid ion exchanger supported nanocomposites: sorption and sensing for environmental applications, *Chem. Eng. J.* 166 (3) (2011) 923–931.
- [50] N. Basavegowda, K. Mishra, Y.R. Lee, Synthesis, characterization, and catalytic applications of hematite (α -Fe₂O₃) nanoparticles as reusable nanocatalyst, *Adv. Nat. Sci. Nanosci. Nanotechnol.* 8 (2) (2017), 025017.
- [51] O. Olsvik, et al., Magnetic separation techniques in diagnostic microbiology, *Clin. Microbiol. Rev.* 7 (1) (1994) 43–54.
- [52] T.C. Yeh, et al., Intracellular labeling of T-cells with superparamagnetic contrast agents, *Magn. Reson. Med.* 30 (5) (1993) 617–625.
- [53] R. Weissleder, et al., Magnetically labeled cells can be detected by MR imaging, *J. Magn. Reson. Imag.* 7 (1) (1997) 258–263.
- [54] A.K. Gupta, A.S. Curtis, Lactoferrin and ceruloplasmin derivatized superparamagnetic iron oxide nanoparticles for targeting cell surface receptors, *Biomaterials* 25 (15) (2004) 3029–3040.
- [55] W. Kemmer, et al., Separation of tumor cells from a suspension of dissociated human colorectal carcinoma tissue by means of monoclonal antibody-coated magnetic beads, *J. Immunol. Methods* 147 (2) (1992) 197–200.
- [56] P. Kronick, R.W. Gilpin, Use of superparamagnetic particles for isolation of cells, *J. Biochem. Biophys. Methods* 12 (1–2) (1986) 73–80.
- [57] K. Sokolov, et al., Real-time vital optical imaging of precancer using anti-epidermal growth factor receptor antibodies conjugated to gold nanoparticles, *Canc. Res.* 63 (9) (2003) 1999–2004.
- [58] C. Chouly, et al., Development of superparamagnetic nanoparticles for MRI: effect of particle size, charge and surface nature on biodistribution, *J. Microencapsul.* 13 (3) (1996) 245–255.
- [59] Y. Zhang, N. Kohler, M. Zhang, Surface modification of superparamagnetic magnetite nanoparticles and their intracellular uptake, *Biomaterials* 23 (7) (2002) 1553–1561.

- [60] A.K. Gupta, A.S. Curtis, Surface modified superparamagnetic nanoparticles for drug delivery: interaction studies with human fibroblasts in culture, *J. Mater. Sci. Mater. Med.* 15 (4) (2004) 493–496.
- [61] M. Zhao, et al., Non-invasive detection of apoptosis using magnetic resonance imaging and a targeted contrast agent, *Nat. Med.* 7 (11) (2001) 1241–1244.
- [62] S. Wada, et al., Antitumor effect of new local hyperthermia using dextran magnetite complex in hamster tongue carcinoma, *Oral Dis.* 9 (4) (2003) 218–223.
- [63] F. Krötz, et al., Magnetofection potentiates gene delivery to cultured endothelial cells, *J. Vasc. Res.* 40 (5) (2003) 425–434.
- [64] E. Augustin, et al., Improved cytotoxicity and preserved level of cell death induced in colon cancer cells by doxorubicin after its conjugation with iron-oxide magnetic nanoparticles, *Toxicol. Vitro* 33 (2016) 45–53.
- [65] G.P. Halliah, K. Alagappan, A.B. Sairam, Synthesis, characterization of CH- α -Fe₂O₃ nanocomposite and coating on cotton, silk for antibacterial and UV spectral studies, *J. Ind. Textil.* 44 (2) (2014) 275–287.
- [66] B. Ahmmad, et al., Green synthesis of mesoporous hematite (α -Fe₂O₃) nanoparticles and their photocatalytic activity, *Adv. Powder Technol.* 24 (1) (2013) 160–167.
- [67] W. Wu, Q. He, C. Jiang, Magnetic iron oxide nanoparticles: synthesis and surface functionalization strategies, *Nanoscale Res. Lett.* 3 (11) (2008) 397.
- [68] M.Y. Nassar, I.S. Ahmed, H.S. Hendy, A facile one-pot hydrothermal synthesis of hematite (α -Fe₂O₃) nanostructures and cephalixin antibiotic sorptive removal from polluted aqueous media, *J. Mol. Liq.* 271 (2018) 844–856.
- [69] H.T. Teo, W.R. Siah, L. Yuliat, Enhanced adsorption of acetylsalicylic acid over hydrothermally synthesized iron oxide-mesoporous silica MCM-41 composites, *J. Taiwan Inst. Chem. Eng.* 65 (2016) 591–598.
- [70] Z. Wei, et al., Facile template-free fabrication of hollow nestlike α -Fe₂O₃ nanostructures for water treatment, *ACS Appl. Mater. Interfaces* 5 (3) (2013) 598–604.
- [71] L.S. Zhong, et al., Self-Assembled 3D flowerlike iron oxide nanostructures and their application in water treatment, *Adv. Mater.* 18 (18) (2006) 2426–2431.
- [72] C.-Y. Cao, et al., Low-cost synthesis of flowerlike α -Fe₂O₃ nanostructures for heavy metal ion removal: adsorption property and mechanism, *Langmuir* 28 (9) (2012) 4573–4579.
- [73] C. Yu, et al., Template-free preparation of mesoporous Fe₂O₃ and its application as adsorbents, *J. Phys. Chem. C* 112 (35) (2008) 13378–13382.
- [74] J. Fei, et al., Large-scale preparation of 3D self-assembled iron hydroxide and oxide hierarchical nanostructures and their applications for water treatment, *J. Mater. Chem.* 21 (32) (2011) 11742–11746.
- [75] V.A. Grover, et al., Adsorption and desorption of bivalent metals to hematite nanoparticles, *Environ. Toxicol. Chem.* 31 (1) (2012) 86–92.
- [76] N.N. Shayan, B. Mirzayi, Adsorption and removal of asphaltene using synthesized maghemite and hematite nanoparticles, *Energy Fuels* 29 (3) (2015) 1397–1406.
- [77] H.I. Adegoke, et al., Adsorption of Cr (VI) on synthetic hematite (α -Fe₂O₃) nanoparticles of different morphologies, *Kor. J. Chem. Eng.* 31 (1) (2014) 142–154.
- [78] X. Wang, et al., Synthesis of β -FeOOH and α -Fe₂O₃ nanorods and electrochemical properties of β -FeOOH, *J. Mater. Chem.* 14 (5) (2004) 905–907.
- [79] S. Bagheri, K. Chandrappa, S. Hamid, Generation of hematite nanoparticles via sol-gel method, *Res. J. Chem. Sci.* 2231 (2013) 606X.
- [80] S. Sahoo, et al., Characterization of γ - and α -Fe₂O₃ nano powders synthesized by emulsion precipitation-calcination route and rheological behaviour of α -Fe₂O₃, *Int. J. Eng. Sci. Technol.* 2 (8) (2010) 118–126.
- [81] J.A. Morales-Morales, Synthesis of hematite α -Fe₂O₃ nano powders by the controlled precipitation method, *Ciencia en Desarrollo* 8 (1) (2017) 99–107.
- [82] J. Borchertding, et al., Iron oxide nanoparticles induce *Pseudomonas aeruginosa* growth, induce biofilm formation, and inhibit antimicrobial peptide function, *Environ. Sci. J. Integr. Environ. Res.: Nano* 1 (2) (2014) 123–132.
- [83] A.A. Bharde, et al., Bacteria-mediated precursor-dependent biosynthesis of superparamagnetic iron oxide and iron sulfide nanoparticles, *Langmuir* 24 (11) (2008) 5787–5794.
- [84] E. Darezereshki, et al., Direct thermal decomposition synthesis and characterization of hematite (α -Fe₂O₃) nanoparticles, *Mater. Sci. Semicond. Process.* 15 (1) (2012) 91–97.
- [85] R.A. Ismail, et al., Antibacterial activity of magnetic iron oxide nanoparticles synthesized by laser ablation in liquid, *Mater. Sci. Eng. C* 53 (2015) 286–297.
- [86] E. Fazio, et al., Iron oxide nanoparticles prepared by laser ablation: synthesis, structural properties and antimicrobial activity, *Colloid. Surface. Physicochem. Eng. Aspect.* 490 (2016) 98–103.
- [87] Y. Fu, et al., Synthesis of large arrays of aligned α -Fe₂O₃ nanowires, *Chem. Phys. Lett.* 379 (3–4) (2003) 373–379.
- [88] P.M. Rao, X. Zheng, Unique magnetic properties of single crystal α -Fe₂O₃ nanowires synthesized by flame vapor deposition, *Nano Lett.* 11 (6) (2011) 2390–2395.
- [89] Y. Yan, et al., One-step self-assembly synthesis α -Fe₂O₃ with carbon-coated nanoparticles for stabilized and enhanced supercapacitors electrode, *Energies* 10 (9) (2017) 1296.
- [90] J. Singh, et al., Preparation and properties of hybrid monodispersed magnetic α -Fe₂O₃ based chitosan nanocomposite film for industrial and biomedical applications, *Int. J. Biol. Macromol.* 48 (1) (2011) 170–176.
- [91] M. Tadic, et al., Magnetic properties of hematite (α -Fe₂O₃) nanoparticles prepared by hydrothermal synthesis method, *Appl. Surf. Sci.* 320 (2014) 183–187.
- [92] K. Rajendran, et al., Biosynthesis of hematite nanoparticles and its cytotoxic effect on HepG2 cancer cells, *Int. J. Biol. Macromol.* 74 (2015) 376–381.
- [93] X. Qu, N. Kobayashi, T. Komatsu, Solid nanotubes comprising α -Fe₂O₃ nanoparticles prepared from ferritin protein, *ACS Nano* 4 (3) (2010) 1732–1738.
- [94] P.T. Anastas, J.C. Warner, Principles of green chemistry, *Green Chem.: Theor. Pract.* (1998) 29–56.
- [95] P. Anastas, J. Warner, *Green Chemistry: Theory and Practice*, Oxford University Press, Oxford, 1998.
- [96] M.F. Al-Hakkani, Biogenic copper nanoparticles and their applications: a review, *SN Appl. Sci.* 2 (3) (2020) 505.
- [97] P.N.V.K. Pallela, et al., Antibacterial efficacy of green synthesized α -Fe₂O₃ nanoparticles using *Sida cordifolia* plant extract, *Heliyon* 5 (11) (2019), e02765.
- [98] H.R. Ali, H.N. Nassar, N.S. El-Gendy, Green synthesis of α -Fe₂O₃ using *Citrus reticulatum* peels extract and water decontamination from different organic pollutants, *Energy Sources Part A Recovery Util. Environ. Eff.* 39 (13) (2017) 1425–1434.
- [99] M.S.H. Bhuiyan, et al., Green synthesis of iron oxide nanoparticle using *Carica papaya* leaf extract: application for photocatalytic degradation of remazol yellow RR dye and antibacterial activity, *Heliyon* 6 (8) (2020), e04603.
- [100] V. Makarov, et al., “Green” nanotechnologies: synthesis of metal nanoparticles using plants, *Acta Naturae* 6 (1) (2014) 35–44.
- [101] I. Ocsy, et al., DNA-guided metal-nanoparticle formation on graphene oxide surface 25 (16) (2013) 2319–2325.
- [102] I. Ocsy, et al., Nanotechnology in plant disease management: DNA-directed silver nanoparticles on graphene oxide as an antibacterial against *Xanthomonas perforans*, *ACS Nano* 7 (10) (2013) 8972–8980.
- [103] P. Wu, et al., Protein-directed synthesis of Mn-doped ZnS quantum dots: a dual-channel biosensor for two proteins, *Chem. Eur. J.* 19 (23) (2013) 7473–7479.
- [104] A. Strayer, et al., Low concentrations of a silver-based nanocomposite to manage bacterial spot of tomato in the greenhouse, *Plant Dis.* 100 (7) (2016) 1460–1465.
- [105] X. He, L. Gao, N. Ma, One-Step instant synthesis of protein-conjugated quantum dots at room temperature, *Sci. Rep.* 3 (1) (2013) 2825.
- [106] H. Shi, et al., One-pot and one-step synthesis of bioactive urease/ZnFe₂O₄ nanocomposites and their application in detection of urea, *Dalton Trans.* 43 (24) (2014) 9016–9021.
- [107] R. Hassanian, D.Z. Husein, M.F. Al-Hakkani, Biosynthesis of copper nanoparticles using aqueous *Tilia* extract: antimicrobial and anticancer activities, *Heliyon* 4 (12) (2018), e01077.
- [108] S. Some, et al., Effect of feed supplementation with biosynthesized silver nanoparticles using leaf extract of *Morus indica* L. V1 on *Bombyx mori* L. (Lepidoptera: bombycidae), *Sci. Rep.* 9 (1) (2019) 14839.
- [109] H.M. Asoufi, T.M. Al-Antary, A.M. Awwad, Green route for synthesis hematite (α -Fe₂O₃) nanoparticles: toxicity effect on the green peach aphid, *Myzus persicae* (Sulzer), *Environ. Nanotechnol. Monit. Manag.* 9 (2018) 107–111.
- [110] S. Amaliyah, et al., Green synthesis and characterization of copper nanoparticles using *Piper retrofractum* Vahl extract as bioreductor and capping agent, *Heliyon* 6 (8) (2020), e04636.
- [111] F. Duman, I. Ocsy, F.O. Kup, Chamomile flower extract-directed CuO nanoparticle formation for its antioxidant and DNA cleavage properties, *Mater. Sci. Eng. C* 60 (2016) 333–338.
- [112] I. Ocsy, et al., A green approach for formation of silver nanoparticles on magnetic graphene oxide and highly effective antimicrobial activity and reusability, *J. Mol. Liq.* 227 (2017) 147–152.
- [113] S.A. Akintelu, et al., Green synthesis of copper oxide nanoparticles for biomedical application and environmental remediation, *Heliyon* 6 (7) (2020), e04508.
- [114] M.F. Al-Hakkani, HPLC analytical method validation for determination of cefotaxime in the bulk and finished pharmaceutical dosage form, *Sustain. Chem. Eng.* (2020) 33–42.
- [115] M.F. Al-Hakkani, Forced degradation study with a developed and validated RP-HPLC method for determination of cefpodoxime proxetil in the bulk and finished pharmaceutical products, *J. Iran. Chem. Soc.* 16 (7) (2019) 1571–1578.
- [116] M.F. Al-Hakkani, Guideline of inductively coupled plasma mass spectrometry “ICP-MS”: fundamentals, practices, determination of the limits, quality control, and method validation parameters, *SN Appl. Sci.* 1 (7) (2019) 791.
- [117] M.F. Al-Hakkani, A rapid, developed and validated RP-HPLC method for determination of azithromycin, *SN Appl. Sci.* 1 (3) (2019) 222.
- [118] M.F. Al-Hakkani, et al., Fully investigation of RP- HPLC analytical method validation parameters for determination of cefixime traces in the different pharmaceutical dosage forms and urine analysis, *Acta Pharmaceutica Scientia* 59 (1) (2020).
- [119] M.d.A. Bezerra, M.A.Z. Arruda, S.L.C. Ferreira, Cloud point extraction as a procedure of separation and pre-concentration for metal determination using spectroanalytical techniques: a review, *Appl. Spectrosc. Rev.* 40 (4) (2005) 269–299.
- [120] S.L. Pal, et al., Nanoparticle: an overview of preparation and characterization, *J. Appl. Pharmaceut. Sci.* 1 (6) (2011) 228–234.
- [121] P.A. Maurice, Applications of atomic-force microscopy in environmental colloid and surface chemistry, *Colloid. Surface. Physicochem. Eng. Aspect.* 107 (1996) 57–75.
- [122] M. Rafique, et al., A review on synthesis, characterization and applications of copper nanoparticles using green method, *Nano* 12 (4) (2017) 1750043.
- [123] M. Ma, et al., Preparation and characterization of magnetite nanoparticles coated by amino silane, *Colloid. Surface. Physicochem. Eng. Aspect.* 212 (2–3) (2003) 219–226.
- [124] S.S. Pareek, K. Pareek, An empirical study on structural, optical and electronic properties of ZnO nanoparticles, *J. Appl. Phys.* 3 (2) (2013) 16–24.
- [125] R. Narayanan, M.A. El-Sayed, Effect of nanocatalysis in colloidal solution on the tetrahedral and cubic nanoparticle shape: electron-transfer reaction catalyzed by platinum nanoparticles, *J. Phys. Chem. B* 108 (18) (2004) 5726–5733.

- [126] D.A. Wollman, et al., High-resolution, energy-dispersive microcalorimeter spectrometer for X-ray microanalysis, *J. Microsc.* 188 (3) (1997) 196–223.
- [127] S. Foner, Versatile and sensitive vibrating-sample magnetometer, *Rev. Sci. Instrum.* 30 (7) (1959) 548–557.
- [128] M. Alagiri, S.B.A. Hamid, Green synthesis of α -Fe₂O₃ nanoparticles for photocatalytic application, *J. Mater. Sci. Mater. Electron.* 25 (8) (2014) 3572–3577.
- [129] D. Nanda, Green synthesis of iron oxide nanostructures, *Chem. Eng.* 1 (2015) 42.
- [130] J.K. Sharma, et al., α -Fe₂O₃ hexagonal cones synthesized from the leaf extract of *Azadirachta indica* and its thermal catalytic activity, *New J. Chem.* 39 (9) (2015) 7105–7111.
- [131] S. Bishnoi, A. Kumar, R. Selvaraj, Facile synthesis of magnetic iron oxide nanoparticles using inedible *Cynometra ramiflora* fruit extract waste and their photocatalytic degradation of methylene blue dye, *Mater. Res. Bull.* 97 (2018) 121–127.
- [132] C. Silveira, et al., Iron-oxide nanoparticles by the green synthesis method using *Moringa oleifera* leaf extract for fluoride removal, *Environ. Technol.* 39 (22) (2018) 2926–2936.
- [133] I. Bibi, et al., Green synthesis of iron oxide nanoparticles using pomegranate seeds extract and photocatalytic activity evaluation for the degradation of textile dye, *J. Mater. Res. Technol.* 8 (6) (2019) 6115–6124.
- [134] M. Jamzad, M.K. Bidkorpeh, Green synthesis of iron oxide nanoparticles by the aqueous extract of *Laurus nobilis* L. leaves and evaluation of the antimicrobial activity, *J. Nanostruct. Chem.* (2020) 1–9.
- [135] E. Rostamizadeh, et al., Green synthesis of Fe₂O₃ nanoparticles using fruit extract of *Cornus mas* L. and its growth-promoting roles in Barley, *J. Nanostruct. Chem.* (2020) 1–6.